INTEGRATED AERODYNAMIC-STRUCTURAL WING DESIGN OPTIMIZATION

by

Eric Robert Unger

Dissertation submitted to the Faculty of the
Virginia Polytechnic Institute and State University
in partial fulfillment of the requirements for the degree of

DOCTOR OF PHILOSOPHY

in

Aerospace Engineering

APPROVED:

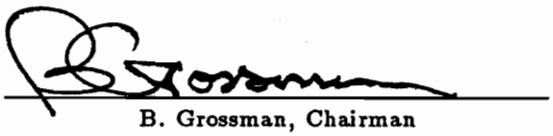

B. Grossman, Chairman

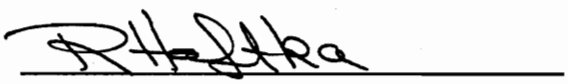

R. T. Haftka

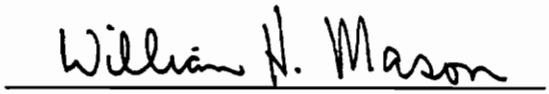

W. H. Mason

R. K. Kapania

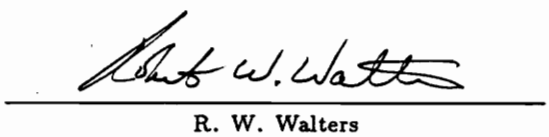

R. W. Walters

March, 1992

Blacksburg, Virginia

INTEGRATED AERODYNAMIC-STRUCTURAL WING DESIGN OPTIMIZATION

by

Eric Robert Unger

Committee Chairman: Bernard Grossman

Aerospace Engineering

(ABSTRACT)

Several procedures for the simultaneous aerodynamic-structural design optimization of aircraft wings are investigated. These procedures include efficient methods for optimization and sensitivity calculations that are applied to two specific design examples. The first is a subsonic transport aircraft with a composite forward-swept wing. The aerodynamic modeling for this case is provided by vortex-lattice theory and the structural model initially utilizes finite-element analyses. Even with efficient sensitivity methods, the approximate optimization problem still requires a large computational effort. To reduce this cost, a variable-complexity model for the structural analyses is introduced. First, an algebraic equation model for wing weight is used in the optimization procedure to obtain an aerodynamic design that approximately accounts for the effects of wing geometry on wing weight. Then this design is refined by simultaneous aerodynamic-structural optimization based on the finite-element analysis. The net effect of this dual structural model is a substantial reduction in optimization costs.

The second example is the wing design of a supersonic High-Speed Civil Transport (HSCT). For this case, the simple wing-weight equations for structures are

retained. For the aerodynamics, a variable-complexity model was introduced with the complex models provided by volumetric wave drag analysis and panel methods. In addition, simple algebraic models for wave and drag due to lift provide inexpensive approximations during most of the optimization cycles. With the minimization of the costly complex sensitivity calculations, a reduction in optimization costs is realized.

ACKNOWLEDGEMENTS

I must confess I wanted to have a deep and poetical way to express my feelings at this point, but I now believe a simple and direct statement is best. To Dr. Bernard Grossman, the best advisor and teacher anyone could want – thanks for everything you have done over the last few years, I would not be here without it. As this work has been group effort, I find myself especially fortunate to work closely with Dr. R.T. Haftka and Dr. W.H. Mason, their advice and insight has been invaluable to this project and my education.

As I stated previously, this work has been a group effort with considerable contributions from other researchers at Va. Tech. and I would be negligent if I did not acknowledge their respective contributions to the project. For finite-element structural analysis on the subsonic transport, I must recognize work by Dr. P-J. Kao and Dr. M. Rais-Rohani. The initial work on the vortex-lattice model and structural interface for the subsonic transport was performed by M. Eppard and D. Polen. My personal contributions to the effort on the subsonic transport centered on improvements to the aerodynamic-structural interface and drag and divergence sensitivity analyses, the development of the optimization problem, the refinement of constraints and move limits, and convergence studies.

For the HSCT I must acknowledge the contributions from M. Hutchison on the wing-weight equations, the drag-due-to-lift analyses, and for the framework of the analysis and sensitivity code. My contribution to the effort was on the implementation of both wave drag models and once again on the development of the optimization problem, constraint, move-limit, and design variable refinement, and convergence studies.

Finally, I have to thank my wife, Susan, for enduring these past few years, especially those times when I have been less than pleasant.

The dissertation is dedicated to my mother.

TABLE OF CONTENTS

LIST OF FIGURES

LIST OF TABLES

LIST OF SYMBOLS

A – Generalized aerodynamic influence matrix

A' – Derivative of the A matrix with respect to p

AR – Aspect ratio

b – Total wing span

c – Local wing chord

c' – Thrust specific fuel consumption

C_D – Drag coefficient

$C_{D_{ft}}$ – Drag coefficient of fuselage and tail

C_{D_i} – Induced drag coefficient

C_{D_v} – Viscous drag coefficient

C_l – Section lift coefficient

C_L – Lift coefficient

C_P – Pressure coefficient

D – Drag

e – Span efficiency

f_1 – Aerodynamic 'black box'

f_2 – Balanced flight equation

f_3 – Structural 'black box'

F_a – Vector of Forces at the load set nodes

F_{aD} – Force at load set nodes at divergence

F_{aG} – Vector of generalized forces

F_{ar} – Force at load set nodes for rigid wing conditions

F_I – Gravitational and inertial force vector

F_z – Lift forces at aerodynamic control points

g_s – Vector of design constraints

I – Identity matrix

J – Jacobian matrix

K_G – Generalized stiffness matrix

L – Lift

M – Mass matrix

n – Load factor

n_m – Number of mode shapes

n_p – Number of design variables

p – Vector of design variables

q – Dynamic pressure

q_D – Divergence dynamic pressure

R – Generalized incremental aerodynamic force vector

R_c – Calculated design aircraft range

R_r – Reference aircraft range

S – Total wing area

S_G – Generalized flexibility matrix

S' – Derivative of generalized flexibility matrix with respect to p

u – Vector of displacements

V_r – Required wing volume

V – Wing volume

W – Total aircraft weight

W_{0r} – Reference aircraft total weight

W_p – Payload weight

W_{uf} – Usable fuel weight

W_w – Design wing weight

W_{wr} – Reference aircraft wing weight

α – Angle of attack

α_r – Rigid angle of attack

Γ – Vorticity vector

Γ_i – Vorticity vector on i^{th} panel

Φ – Vector of mode shapes

θ – Vector of generalized displacements

ξ, η – normalized coordinates

1. INTRODUCTION

The goal of any aircraft design is to strike a balance between the demands placed upon the vehicle by aerodynamics, structures, controls, and propulsion. Since improvements in any given characteristic frequently degrade others, the required balance is difficult to achieve without accounting for interdisciplinary interactions. Unfortunately, traditional design practice limits the inclusion of these interdisciplinary effects to the initial or *conceptual* phase of the design process. If the interactions that are present in the aircraft are minimal (or can at least be minimized), this design technique can be quite successful, as evidenced by the vast number of successful aircraft that exist today. However, one could conjecture that such designs would be even more efficient if interdisciplinary effects are included into the more detailed levels of design. Such efficiency gains are part of the motivation behind the recent interest into multidisciplinary design techniques that account for interdisciplinary interactions. Additional motivation is provided by the introduction of composite materials which permit extensive aeroelastic tailoring, as well as the requirements of advanced vehicles, such as the aerospace plane, where because of extreme flight conditions, the interdisciplinary interactions are particularly important.

One of the more important interdisciplinary interactions in modern aircraft design is that of aerodynamics and structures. One aspect of that interaction is the use of composite materials to tailor the deformation of aircraft wings so as to affect aerodynamic loads. This so-called aeroelastic tailoring is the focus of many publications (see [1,2] for reviews of the state of the art). Aeroelastic tailoring is particularly important for forward-swept-wing aircraft, where geometric influences result in an unfavorable bend-twist coupling known as *wash-in*, and lead to aeroelastic instabilities.

Aeroelastic tailoring is a limited form of integrated design, as the structure is designed to affect aerodynamic properties, but the aerodynamic design does not consider structural constraints except in a very broad sense (such as in limits on wing aspect ratio and thickness). In [3] it has been shown that in an integrated design process, it may be reasonable to use a suboptimal aerodynamic design if it results in reduced structural weight, because the weight savings may be converted into improved aerodynamic efficiency.

Past work has considered the integrated aerodynamic-structural design optimization problem. Early work by McGeer [4], considered the selection of a distribution of lift, chord, and thickness to minimize induced drag with a number of practical constraints placed on simple models of aerodynamics and structures. Initial work at Virginia Tech [4], began with the integrated design of a sailplane wing utilizing simple lifting-line aerodynamics in conjunction with beam theory for the structural analysis and then progressed to utilize vortex-lattice aerodynamics and finite-elements for the structures [5]. Subsequent work [6,7], also included vortex-lattice theory and finite-element methods for the design of a transport wing. Similar work by Gallman, Kroo, and Smith [8], considered the design of a joined-wing transport utilizing vortex-lattice and beam theory for the aerodynamic and structural

analysis respectively. Additional work on transport aircraft has been considered by Wrenn and Dovi in [9], where the optimization was broken down into multiple levels of design complexity utilizing simple aerodynamic models and finite-element theory for the structures (in the more detailed design levels). Further work with aerodynamic-structural optimization can be found in [10] where Malone and Mason utilized simple analytic methods to perform parametric design studies of aircraft. The addition of active control systems has been considered in work by Livne, Friedmann, and Schmit [11,12], with kernel-function aerodynamics and equivalent plate theory for the structures. More generalized multi-disciplinary work, along with efficient methods for obtaining system sensitivities was considered by Sobieski in [13,14].

The present work provides a generalized treatment to the integrated aerodynamic-structural design problem. The systematic approach addresses the prohibitive computational costs of multi-disciplinary design with some of the analysis and optimization techniques available today. The first of these methods involves a dramatic reduction to the cost sensitivity analysis through the use of modular sensitivity analysis [13,14]. An example of the modular technique with aerodynamic, structural, and active control influences was considered in [15]. Additional savings in computational effort are achieved by making use of both detailed numerical models and simple algebraic expressions traditionally employed at the conceptual design phase. This method of a dual level of complexity in the analysis is called here *variable-complexity modeling.*

Chapter 2 outlines the analysis required for the generalized aeroelastic analysis procedure. The structural and aerodynamic response of the wing are represented in a functional form and methods to solve the complex coupled system are discussed.

In addition, the evaluation of aeroelastic divergence instability is discussed. Chapter 3 presents the evaluation of system response derivatives which are necessary for optimization. These derivatives are obtained efficiently with the utilization of the aforementioned modular sensitivity approach. Chapter 4 introduces the sequential approximate optimization and variable-complexity modeling as a means to reduce the computational burden of the multidisciplinary design problem. The remaining chapters demonstrate the practical application of the methods presented. Design case 1, presented in chapter 5, is the combined aerodynamic-structural design optimization of a subsonic transport aircraft. This case provides a detailed example of modular-sensitivity analysis and an introduction to variable-complexity modeling. The second design example, presented in chapter 6, illustrates the aerodynamic design of a High-Speed Civil Transport (HSCT) utilizing a substantial amount of variable-complexity modeling.

2. ANALYSIS

The ability to effectively represent the coupled structural and aerodynamic response of the wing is essential to completely model the design process. The method presented below provides such a representation in a generalized formulation to allow for a broad range of analysis methodology. Additional information on the solution of aeroelastic systems can be found in Refs. [17] and [18].

2.1. Aeroelastic Formulation

The equations of equilibrium obtained from a finite-element structural model of the wing are

$$Ku = F_a + F_I \,, \tag{2.1}$$

where K is the stiffness matrix, u is the displacement vector, F_a represents the applied aerodynamic loads, and F_I gives the inertial loads. To reduce the cost of the aeroelastic analysis, (in particular the cost of derivatives of aerodynamic loads with respect to structural deformations) it is advantageous to decrease the number of degrees of freedom in the structural model. Such a reduction can be

realized by utilizing a reduced-basis structural analysis. To employ this approach the displacement vector is approximated as

$$u = \Phi\theta\,, \tag{2.2}$$

where Φ the mode-shape matrix composed of n_m deformation shapes and θ is a vector of modal magnitudes defined as the generalized displacements. Since a system that may have hundreds or even thousands of degrees of freedom may be adequately represented with perhaps twenty of thirty mode shapes (vibration modes are commonly utilized), a clear advantage can be obtained using this approximation. The modes are usually made orthonormal with respect to a matrix M (mass matrix in the case of vibration modes), that is

$$\Phi^T M \Phi = I\,. \tag{2.3}$$

This approximation is substituted into Eq. (2.1) and the resulting equations are premultiplied by Φ^T to yield the reduced structural system as

$$\Phi^T K \Phi\theta \equiv K_G\theta = \Phi^T(F_a + F_I) \equiv F_{aG} + F_{IG}\,, \tag{2.4}$$

where $K_G = \Phi^T K \Phi$ is the generalized stiffness matrix and $\Phi^T F_a$ is the generalized aerodynamic force vector denoted as F_{aG}, with F_{aG_i} being the work done by the aerodynamic loads on the ith mode.

The loads, F_a, are determined from an aerodynamic analysis procedure. It is assumed that these aerodynamic forces are dependent on some set of design parameters, p, the root angle of attack, α, (which we assume to represent the only body contribution), and the vector of generalized displacements, θ. The load vector F_a is then obtained as

$$F_{aG} = f_1(p, \alpha, \theta)\,. \tag{2.5}$$

The angle of attack, α, is determined for a given flight condition from the requirement that α is sufficient to provide an F_{aG} that provides the required lift

$$f_2(p, F_{aG}) = nW - N^T F_a = 0\,, \tag{2.6}$$

where N is a summation vector ($N^T F_a$ gives the total vertical forces on both wings), n is the load factor, and W is the weight of the aircraft. To transform this equation to generalized coordinates we approximate F_a as

$$F_a \cong M\Phi F_{aG}\,. \tag{2.7}$$

This approximation is consistent with that of Eq. (2.3) in that if we multiply Eq. (2.7) by Φ^T, we find that it is satisfied exactly. Then Eq. (2.6) can be written as

$$f_2(p, F_{aG}) = nW - \hat{N}^T F_{aG} = 0\,, \tag{2.8}$$

where

$$\hat{N}^T = N^T M\Phi\,. \tag{2.9}$$

The vector of generalized displacements, θ, can also be represented functionally as

$$\theta = f_3(p, F_{aG})\,, \tag{2.10}$$

with f_3 representing the solution of Eq. (2.4).

2.2. Solution Procedure

With the structural and aerodynamic response of the wing in functional form it is now necessary to solve the static system for a given flight condition. Inspection of Eqs. (2.5), (2.8), and (2.10) reveals a set of coupled, generally nonlinear equations for the vector of generalized aerodynamic loads, F_{aG}, the wing-root angle of attack,

α, and the vector of generalized displacements, θ. For the analysis problem, the vector of design parameters, p, may be considered to be specified. In [13] and [14], Sobieski presents a modular approach for the evaluation of sensitivity derivatives in such coupled interdisciplinary equations. This modular approach allows the individual discipline analysis procedures to be treated as *black boxes* that do not need to be changed during the coupling procedure. Here we are interested in solving the coupled system with a Newton's Method that will require cross-disciplinary sensitivities. Therefore a modular approach similar to [13] and [14] may also be applied to the analysis problem with f_1 representing an *aerodynamic black box* and f_3 a *structural black box.*

The solution to the system begins by setting up the system in homogeneous form,

$$F_{aG} - f_1(p, \alpha, \theta) = 0\,, \tag{2.11}$$

$$-f_2(p, F_{aG}) = \hat{N}^T F_{aG} - nW(p) = 0\,, \tag{2.12}$$

$$\theta - f_3(p, F_{aG}) = 0\,. \tag{2.13}$$

Then, an initial estimate for angle of attack, α^0, the generalized forces, F^0_{aG}, and the generalized deflections, θ^0, is made. That estimate can be improved by using Newton's method. The iterative process may be written as

$$J\Delta Y = \Delta f\,, \tag{2.14}$$

where

$$\Delta Y = \left\{ \begin{array}{c} \Delta F_{aG} \\ \Delta\alpha\,, \\ \Delta\theta \end{array} \right\}\,, \tag{2.15}$$

and

$$\Delta f = \begin{Bmatrix} f_1(p, \alpha^0, \theta^0) - F^0_{aG}\,, \\ f_2(p, F^0_{aG}) \\ f_3(p, F^0_{aG}) - \theta^0 \end{Bmatrix}\,, \tag{2.16}$$

and the Jacobian J is given, (for the balanced flight condition), as

$$\begin{aligned} J &= \begin{bmatrix} I & -\partial f_1/\partial\alpha & -\partial f_1/\partial\theta \\ -\partial f_2/\partial F_{aG} & 0 & 0 \\ -\partial f_3/\partial F_{aG} & 0 & I \end{bmatrix}\,, \\ &= \begin{bmatrix} I & -qR & -qA \\ \hat{N}^T & 0 & 0 \\ -S_G & 0 & I \end{bmatrix}\,. \end{aligned} \tag{2.17}$$

The Jacobian contains the dynamic pressure q, the generalized incremental aerodynamic force vector, qR, the generalized aerodynamic influence coefficient matrix, qA, and the generalized flexibility matrix S_G. The incremental aerodynamic force vector is defined such that its component qr_i represents the ith generalized aerodynamic force due to a unit change in α, and the aerodynamic influence coefficient matrix, is defined such that its component qa_{ij} represents the ith generalized force due to a unit change in θ_j. Similarly, the generalized flexibility matrix, is such that s_{ij} is the change in θ_i due to a unit change in F_{aG_j}, and from Eq.(2.4) $S_G = K_G^{-1}$. In many cases the matrix A has to be calculated by using finite differences, that is perturbing each θ_i and recalculating f_1. This makes the calculation of A the most expensive part of the Jacobian evaluation.

Partial solution of Eq. (2.14) yields the following three equations for the increments $\Delta\theta$, $\Delta\alpha$ and ΔF_{aG}:

$$(I - qS_G A^x)\Delta\theta = S_G B\Delta f_1 + \frac{S_G R}{\hat{N}^T R}\Delta f_2 + \Delta f_3\,, \tag{2.18}$$

$$\Delta\alpha = \frac{\Delta f_2 - \hat{N}^T\Delta f_1 - q\hat{N}^T A\Delta\theta}{q\hat{N}^T R}\,, \tag{2.19}$$

$$\Delta F_{aG} = \Delta f_1 + qR\Delta\alpha + qA\Delta\theta\,, \tag{2.20}$$

where we define

$$B \equiv I - \frac{R\hat{N}^T}{\hat{N}^T R}\,, \tag{2.21}$$

and

$$A^x \equiv B\,A\,. \tag{2.22}$$

Also important to the analysis problem is the evaluation of the aeroelastic divergence instability. This condition is evaluated at a fixed angle of attack, because it can be assumed the pilot does not react fast enough to change the angle of attack as the wing diverges. The instability is characterized by a homogeneous solution to Eq. (2.14) not including $\Delta\alpha$ and the weight balance equation, that is

$$\begin{bmatrix} I & -qA \\ -S_G & I \end{bmatrix} \begin{Bmatrix} \Delta F_{aG} \\ \Delta\theta \end{Bmatrix} = 0\,. \tag{2.23}$$

Equation (2.23) is an eigenvalue problem for q. The lowest eigenvalue is the divergence dynamic pressure q_D. We denote the corresponding eigenvector as $[F_{aGD}, \theta_D]^T$. Equation (2.23) can be reduced to a standard linear eigenproblem by substituting for $\Delta\theta$ in terms of ΔF_{aG} to obtain

$$(AS_G - \frac{1}{q}I)\Delta F_{aG} = 0\,. \tag{2.24}$$

In the present aeroelastic divergence analysis only the wing is modeled, neglecting the effect of interaction with the fuselage. This effect may be of consequence for forward-swept wings, *e.g.* Rodden, [20,21].

3. SENSITIVITY CALCULATION

During a design procedure it is necessary to evaluate the derivatives (or sensitivities) of the system response with respect to a vector of design parameters p. These sensitivities could be evaluated by differentiating Eqs. (2.18), (2.19), and (2.20) (*e.g.*, [4]). However, this approach requires the calculation of derivatives of the matrices A and S_G which can be very costly. Here, instead, we follow [13] and [14] and utilize a modular approach by differentiating Eqs. (2.5), (2.8) and (2.10) with respect to p to obtain

$$JY' = f' , \tag{3.1}$$

where a prime denotes differentiation with respect to p and where

$$Y' = [\, F'_{aG} \quad \alpha' \quad \theta' \,]^T , \tag{3.2}$$

and

$$f' = [\, f'_1 \quad f'_2 \quad f'_3 \,]^T , \tag{3.3}$$

along with the definition $f'_i \equiv \partial f_i / \partial p$, for $i = 1, 2, 3$. The Jacobian, J, appearing in Eq. (3.1) is the same as that used in the analysis procedure and is defined by

Eq. (2.17). Equation (3.1) can be partially solved to yield

$$(I - qS_G A^x)\theta' = S_G B f_1' + \frac{S_G R}{\hat{N}^T R} f_2' + f_3' , \tag{3.4}$$

$$\alpha' = \frac{f_2' - \hat{N}^T f_1' - q\hat{N}^T A\theta'}{q\hat{N}^T R} , \tag{3.5}$$

$$F_{aG}' = f_1' + qR\alpha' + qA\theta' , \tag{3.6}$$

where B and A^x are defined in Eqs.(2.21) and (2.22) respectively. This approach does not require any derivatives of A and S_G but only partial derivatives of f_1, f_2 and f_3. For example, f_1' denotes the derivative of F_{aG} with respect to a design variable when α and θ are fixed.

To find the derivative of the divergence dynamic pressure q_D with respect to a design parameter p, we differentiate Eq. (2.23) at $q = q_D$ with respect to p

$$\begin{bmatrix} I & -q_D A \\ -S_G & I \end{bmatrix} \begin{Bmatrix} F_{aGD}' \\ \theta_D' \end{Bmatrix} + \begin{bmatrix} 0 & -(q_D A)' \\ -S_G' & 0 \end{bmatrix} \begin{Bmatrix} F_{aGD} \\ \theta_D \end{Bmatrix} = 0 . \tag{3.7}$$

We premultiply Eq. (3.7) by the left eigenvector of Eq. (2.23), $[F_{aGL}^T, \theta_L^T]$, defined by

$$[F_{aGL}^T, \theta_L^T] \begin{bmatrix} I & -q_D A \\ -S_G & I \end{bmatrix} = 0 , \tag{3.8}$$

and obtain

$$[F_{aGL}^T, \theta_L^T] \begin{bmatrix} 0 & -(q_D A)' \\ -S_G' & 0 \end{bmatrix} \begin{Bmatrix} F_{aGD} \\ \theta_D \end{Bmatrix} = 0 , \tag{3.9}$$

or

$$q_D' = -\frac{q_D F_{aGL}^T A' \theta_D + \theta_L^T S_G' F_{aGD}}{F_{aGL}^T A \theta_D} . \tag{3.10}$$

Equation (3.10) contains derivatives of A and S_G with respect to p which we have previously managed to avoid. However, the corresponding terms can be simplified. Using the definition of A, Eq. (2.17), we note that

$$qA'\theta_D = \frac{\partial}{\partial p}\left(\frac{\partial f_1}{\partial \theta}\right)\theta_D . \tag{3.11}$$

To see how $A'\theta_D$ can be calculated without obtaining A' consider a more generic case. Let f be a function of a vector X, and let D be a given unit vector. Let X_0 be a particular choice for X, then the scalar product of the gradient $\partial f/\partial X$ at X_0 and the vector D, is the directional derivative of f in the direction D, that is

$$\begin{aligned}\frac{\partial f}{\partial X}\Big|_{X_0} D &= \lim_{\epsilon \to 0} \frac{1}{\epsilon} [f(X_0 + \epsilon D) - f(X_0)] \\ &= \frac{d}{d\epsilon}[f(X_0 + \epsilon D)]_{\epsilon=0} . \end{aligned} \tag{3.12}$$

It is easy to check that Eq. (3.12) holds even if D is not a unit vector, but has arbitrary magnitude. Equation (3.12) provides us with a way of calculating the product $\partial f/\partial X$ times D without calculating the individual components of $\partial f/\partial X$. If we now consider Eq. (3.11) and use θ as the vector X and θ_D as the vector D we can write for each component f_{1_i}

$$\left(\frac{\partial f_{1_i}}{\partial \theta}\right) \theta_D = \frac{d}{d\epsilon}[f_{1_i}(\theta_0 + \epsilon\theta_D)]_{\epsilon=0} , \tag{3.13}$$

where θ_0 is the nominal value of θ, and the index i, varies from 1 to n_m. Note that $\partial f_{1_i}/\partial\theta$ is a row vector with elements composed of the derivatives of f_{1_i} with respect to the individual components of θ. Equation (3.13) can also be written as

$$\left(\frac{\partial f_1}{\partial \theta}\right) \theta_D = \frac{d}{d\epsilon}[f_1(\theta_0 + \epsilon\theta_D)]_{\epsilon=0} , \tag{3.14}$$

where $\partial f_1/\partial\theta$ is a matrix whose ith row is $\partial f_{1i}/\partial\theta$. The right-hand side is typically calculated by finite differences which involves two calculations of f_1. Then a finite-difference derivative with respect to p involves n_p more calculations of f_1 at perturbed values of p (n_p is the number of design variables). This compares with $n_m \times n_p + 1$ calculations of f_1 to obtain A' by finite differences.

The term $S'F_{aGD}$ is easier for two reasons. First, it is not very expensive to calculate K'_G by finite differences and also since $S_G = K_G^{-1}$

$$S'_G = -S_G K'_G S_G . \tag{3.15}$$

4. OPTIMIZATION PROCEDURE

The multi-disciplinary wing optimization can be formulated as

$$\begin{aligned} &\textit{minimize} && f(p)\,, \\ &\textit{such that} && g_s(p) \geq 0\,, \\ & && g_a(p) \geq 0\,, \\ & && g_p(p) \geq 0\,, \end{aligned} \tag{4.1}$$

where p is the vector of design parameters and g_s represents the structural constraints, g_a the aerodynamic constraints, and g_p the performance constraints. The objective function, $f(p)$, could represent any property of the aircraft, although it is common to minimize weight or cost.

While it would be possible to provide an optimization algorithm with the relations required to solve the aeroelastic problem (which would provide the information needed for the constraint analysis), the cost to obtain solutions to the system several hundred times would be prohibitive. This difficulty is avoided with the use of approximate optimization procedures outlined in the following sections.

4.1. Sequential Approximate Optimization

In this approach, a sequence of approximate optimization problems or cycles is solved. At the beginning of each of these cycles, expensive constraints are approximated and an approximate set of constraints is generated. The most common form of this approximation is a simple linearization where the approximate set of constraints takes the form

$$\tilde{g}(p) = g(p_0) + \frac{\mathrm{d}g}{\mathrm{d}p}(p_0)\,(p - p_0)\,, \tag{4.2}$$

where $\tilde{g}(p)$ represents a set of approximate constraint functions and $g(p_0)$ represents the exact set at the initial design point p_0. The expense of this frequently used approach lies in the derivative evaluations. However, if Newton's method is used to solve the aeroelastic system, the Jacobian containing the required sensitivity terms is available.

In many circumstances a constraint is a function of several terms, some may be trivial to calculate while others may be expensive. For such constraints, it makes sense to linearize the expensive terms as opposed to the entire constraint to yield a better approximation. As an example consider the calculation of aircraft range. Range is dependent on the design parameters, (which presumably define the fuel, payload, wing area, altitude, etc.), the aircraft weight, and the aircraft drag. Functionally the range is given as

$$R_c = R_c(p, W, D)\,, \tag{4.3}$$

where W is the weight and D is the drag. The drag is considerably more expensive to calculate than the weight and should be linearized. The approximate range used here is given as

$$\tilde{R}_c = R_c(p, W, \tilde{D})\,, \tag{4.4}$$

where

$$\tilde{D}(p) = D(p_0) + \frac{\mathrm{d}D}{\mathrm{d}p}(p_0)\,(p - p_0)\ . \tag{4.5}$$

The approximate optimization problem is solved to produce an approximate optimum, and the process is called an optimization *cycle.* It is assumed that at design points far away from the initial design, the approximations will become inaccurate. Thus it is necessary to apply *move limits* on the design variables. That is, the optimization procedure will not be allowed to change design variables beyond prescribed upper and lower bounds,

$$p_l^i \leq p^* \leq p_u^i\ , \tag{4.6}$$

where p^* represents the cycle optimum, p_l^i is the lower design bound for the i^{th} cycle, and p_u^i give the upper bound on the same cycle.

The result of one optimization cycle is used as the initial design point for another approximate optimization and the cycle is repeated until convergence. The number of cycles required for convergence and the size of the move limits is highly dependent on the individual problem and experimentation is often necessary.

4.2. Variable-Complexity Modeling

Variable-complexity modeling involves combining generally expensive detailed or complex numerical analysis with simple algebraic expressions that capture the behavior of the detailed models. This dual-model approach is utilized during the optimization sequence in two methods. The first of these methods is illustrated in chapter 5, and involves the coupling of detailed analysis for one discipline and simple analysis for the other. In this example, a simple equation model of structural weight is first used in a numerical optimization sequence to obtain an aerodynamic

design which approximately accounts for structural effects. Then, this design is refined with integrated aerodynamic-structural optimization using detailed models for both aerodynamics and structures.

The second method of variable-complexity modeling involves the use of simple models to approximate the behavior of the detailed models during the optimization cycles. This type of modeling is demonstrated extensively in chapter 6, where algebraic models for wave drag and drag due to lift are utilized during optimization in addition to the detailed numerical methods.

4.2.1. Scaled approximation

With scaled approximation, linearized approximations are replaced with simple models which capture the behavior of the more exact detailed calculations over the global design space. While such simple models capture correct behavior in the global sense, they may not be particularly accurate at a local design point and require a suitable scaling factor, β, which is defined as the ratio between the detailed and simple models:

$$\beta(p_0) = \frac{f_d(p_0)}{f_s(p_0)} . \tag{4.7}$$

where p_0 is the initial design point, f_d represents the result from the complex or detailed model and f_s gives the result from the simple or global-approximation model. Note that this scaling factor is held constant during a given optimization cycle.

The advantage of such an approach is twofold. First, the simple models generally do not catastrophically break down far from the linearization point like locally linearized approaches can. The consequence of this behavior is the ability to use larger move limits during a given optimization cycle. The second advantage of

this method is that sensitivity terms may be computed very inexpensively from the simple models.

4.2.2. Global-Local Approximation

Another form of Variable Complexity Modeling which shows promise is the combination of the local and global approximations. The following is a brief description of one such method called here *Global-Local* Approximation (GLA).

As previously mentioned the scaling factor β is held constant during a optimization cycle in the scaled procedure. It is possible to use sensitivity information from the detailed model to vary the scaling factor, [22,23]. In this case the scaling factor is given as

$$\beta(p) = \beta(p_0) + \beta'(p_0)(p - p_0)\,, \tag{4.8}$$

where β' is the derivative of the scaling factor with respect to the design variables. Equation (4.8) can be written as

$$\beta(p) = \frac{f_d(p_0)}{f_s(p_0)}\left[1 + (p - p_0)\left(\frac{f_d'(p_0)}{f_d(p_0)} - \frac{f_s'(p_0)}{f_s(p_0)}\right)\right], \tag{4.9}$$

where f_d' represents the detailed model sensitivity, and f_s' the simple model sensitivity. The advantage of this method is that it allows a further increase in move limits if accurate derivatives can be obtained. A disadvantage of the method is that it requires the use of costly detailed model sensitivities.

5. DESIGN CASE 1: SUBSONIC TRANSPORT

First we consider the design of a forward-swept composite wing for a subsonic transport aircraft. The design of the wing was formulated so as to reduce the weight of the aircraft while maintaining a given range. The wing-design problem requires properties for the rest of the aircraft, which are obtained from a reference transonic transport design, described in Table 5.1 and Ref. [24]. Due to the overwhelming computational costs associated with using non-linear transonic aerodynamics in numerical optimization procedures, the cruise Mach number was reduced from 0.78 to 0.68 to allow for the use of a compressibility-corrected vortex-lattice method, as in [6]. Furthermore, the aft-swept wing of the reference aircraft was replaced with a forward-swept wing to allow for natural laminar flow over a substantial portion of the wing, (which can be realized for moderate forward sweep).

5.1. Forward-Swept-Wing Design Problem

The objective function to be minimized for this design problem is the gross weight of the aircraft W given as

$$W = W_s + W_{uf} + W_p \,, \tag{5.1}$$

Table 5.1. Reference Subsonic Transport Specifications [24]

Weight, N:		
	W_{gw}	449,400
	W_{rs}	285,200
	W_{uf}	27,380
	W_p	136,800
	W_{rw}	30,200
Wing:		
	Aspect ratio	14
	Area, m^2	83.98
	Span, m	34.29
	Thickness	12%
	Sweep	15°
	Taper Ratio	.25
Av. Cruise:		
	Mach No.	.78
	C_L	.672
	L/D	20.7
	Specific Fuel Consumption	.430
Range, m:		2.34×10^6

where W_s is the aircraft standard empty weight, W_{uf} is the usable fuel weight, and W_p is the payload weight. The payload weight is taken to be the same as for the reference aircraft. The usable fuel weight is a design variable adjusted by the optimization procedure so as to satisfy the range requirement. The standard empty weight of the aircraft, W_s, is calculated from the standard empty weight of the reference aircraft, W_{rs}, by assuming that structural weight savings in the wing are amplified by a growth factor η due to corresponding savings in non-structural weight and in the tail and fuselage. That is

$$W_s = W_{rs} - \eta\,(W_{rw} - W_w)\,, \tag{5.2}$$

where W_{rw} and W_w are the structural weight of the wings of the reference and

design aircraft, respectively and η was selected to be 2.8. This value is arrived at by assuming that 50% of a wing's total weight is non-structural and that every pound of total wing weight contributes an additional 0.4 lbs. of fuselage and tail weight [25]. For this calculation, the structural wing weight of the design aircraft was calculated by summing up the weights of the structural members.

The wing structure was designed to withstand a 2.5g pull-up maneuver with a 1.5 factor of safety. This maneuver was assumed to follow an altitude loss, and occurs at 2.5 times the cruise dynamic pressure. The wing skin was made of 0-deg, $\pm$45-deg, and 90-deg graphite-epoxy laminate with the zero direction being a design parameter used to create favorable bending-twist coupling to prevent aeroelastic divergence. Maximum strain constraints of 0.012 in the fiber and normal direction and in shear were imposed on each ply. These strain allowables are very high and are based on expected properties of future advanced composite materials. Spar caps were made of unidirectional material with a maximum stress capacity of 0.262 GPa. This flexible structure was modeled by a finite-element model shown in Fig. 5.1. The wing was required to have an aeroelastic divergence dynamic pressure larger than 1.2 times the dynamic pressure at the pull-up maneuver.

The aerodynamic design was primarily controlled by the requirement for the range to be equal to that of the reference aircraft (2340 Km). The aerodynamic loads were calculated using a vortex lattice-model with 120 panels. The airfoil section used for all spanwise stations was a natural laminar-flow airfoil designated as $HSNLF(1) - 0213$, described in [26].

Table 5.2 lists the design variables used for the optimization procedure. The first 6 variables are planform design variables shown in Figure 5.2. The next two variables are twist angle variables that define the wing twist before structural deformations are included, thus defining a *jig shape*.

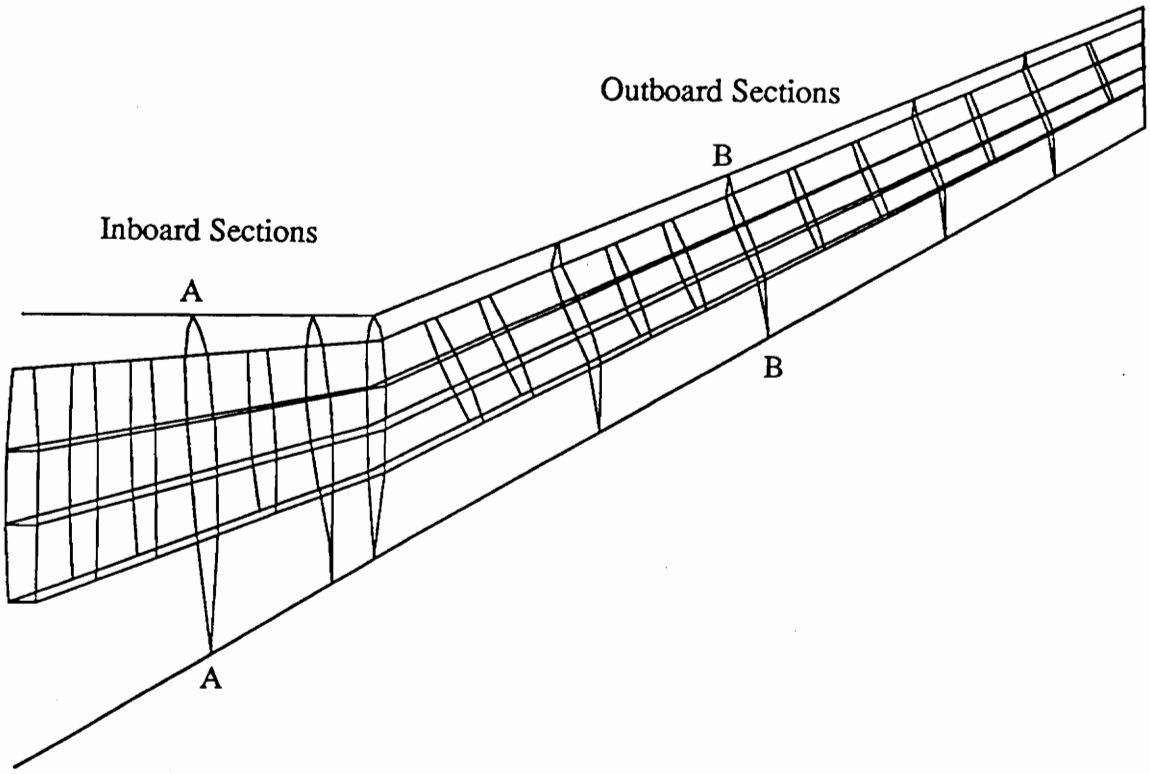

Figure 5.1. Structural Layout of the Subsonic Design Wing

The two performance variables listed in Table 5.2 affect mostly the range. The cruise dynamic pressure is a surrogate for the cruise altitude and, together with the usable fuel, is selected so as to achieve the desired range at minimum weight.

There are 24 structural design variables which define the thickness of the zero, ninety, and forty-five degree plies. The wing is divided into four regions—two in the inboard box, (see Fig. 5.1) and two in the outboard box. The line A–A in Figure 5.1 marks the division of the inboard box and the line B–B marks the division of the outboard box. The ply thicknesses are taken to be constant in each region, making for 12 variables for the lower skin and 12 variables for the upper skin. Four design variables control the cross-sectional areas of the two front and two rear spar caps. Finally, one design variable is used to control the zero direction for the laminate for both lower and upper skins.

Table 5.2. Design Variables for Subsonic Transport

8 Geometric Design Variables	1. Root chord 2. Break chord 3. Tip chord 4. Root to break 5. Break to tip 6. Sweep angle 7. Twist angle at break 8. Twist angle at tip
2 Performance Design Variables	9. Cruise dynamic pressure 10. Usable fuel weight
29 Structural Design Variables	11.–34. Ply thicknesses 35.–38. Spar-cap areas 39. Ply orientation

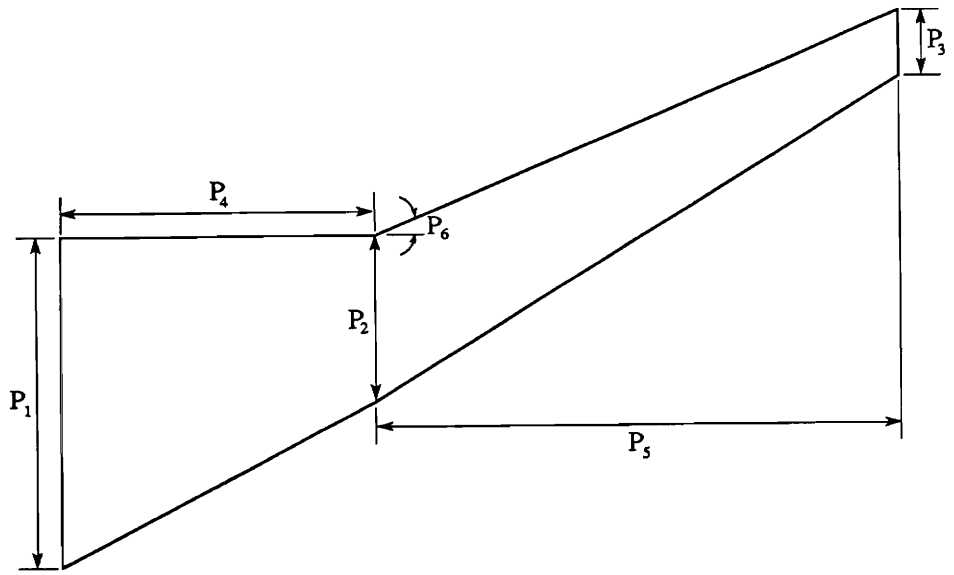

Figure 5.2. Subsonic Transport Planform Design Variables

The constraints used in the present optimization are listed in Table 5.3 and consist of the strain, stress, aeroelastic divergence, fuel volume, and range constraints discussed above along with a landing speed and a local stall constraint imposed on the design problem. The two final constraints were added when preliminary optimization results showed that the wing area was becoming very small. The first of these constraints is a landing speed maximum of 150 knots at 5000 ft. altitude, with an assumed maximum lift coefficient of 1.5 (flaps deployed). This constraint significantly affects the design by imposing a lower bound on the wing area for a given gross weight. The second constraint limits the lift coefficient of the outboard wing section to 1.0 during cruise. In these sections the chords tend to get very small during optimization, thus forcing the local lift coefficients to enter a stall regime. The addition of the constraint effectively prevents the optimizer from allowing this to occur.

Table 5.3. Design Constraints for Subsonic Transport

305 Structural Constraints	1.–228. Max. skin strain 229.–304. Max. spar-cap stress 305. Divergence dynamic pressure
4 Performance Constraints	306. Range 307. Fuel volume 308. Landing speed 309. Outboard section C_L

5.2. Subsonic Analysis

For this example, a given set of 48 points, called here the *load set nodes*, were selected for the aeroelastic analysis. These nodes were used to define mode shapes comprising a value of unity at one of the load-set nodes and zero elsewhere. With this particular set of mode shapes, the generalized displacements give the value of the vertical deflection at each of load set nodes, and the generalized forces give the value of the forces at each of these nodes.

The generalized forces were evaluated by interpolating the wing deflections to the aerodynamic control points, evaluating the vertical aerodynamic loads, and transferring these forces to the load set nodes. The vertical aerodynamic loads, are determined from a vortex-lattice method (*e.g.*, [27]), which is utilized to compute the lift and induced drag. The wing is discretized into panels, with each panel containing an element of a horseshoe vortex of strength γ_j (see Fig. 5.3). By enforcing flow tangency at each panel, a vector of circulation strengths Γ is computed from the wing geometry, which depends upon p, the vector of design parameters, along with the vector of vertical displacements, θ, and the angle of attack, α. The aerodynamic forces are computed from a local application of the Kutta-Joukowski theorem, and compressibility effects are included through a Göthert transformation. Figure 5.4 shows an example wing with load set nodes and sample vortex-lattice control points.

The vertical displacements at the load set are calculated by finite-element analysis using a modification of the WIDOWAC program, [28]. First the nodal-displacement vector u is calculated from the aerodynamic loads and the gravitational and inertial loads. The vertical displacements at the load set θ are then extracted from u. The generalized flexibility matrix, S_G, was calculated by applying a unit load at one load-set node and solving for the displacements at the other nodes.

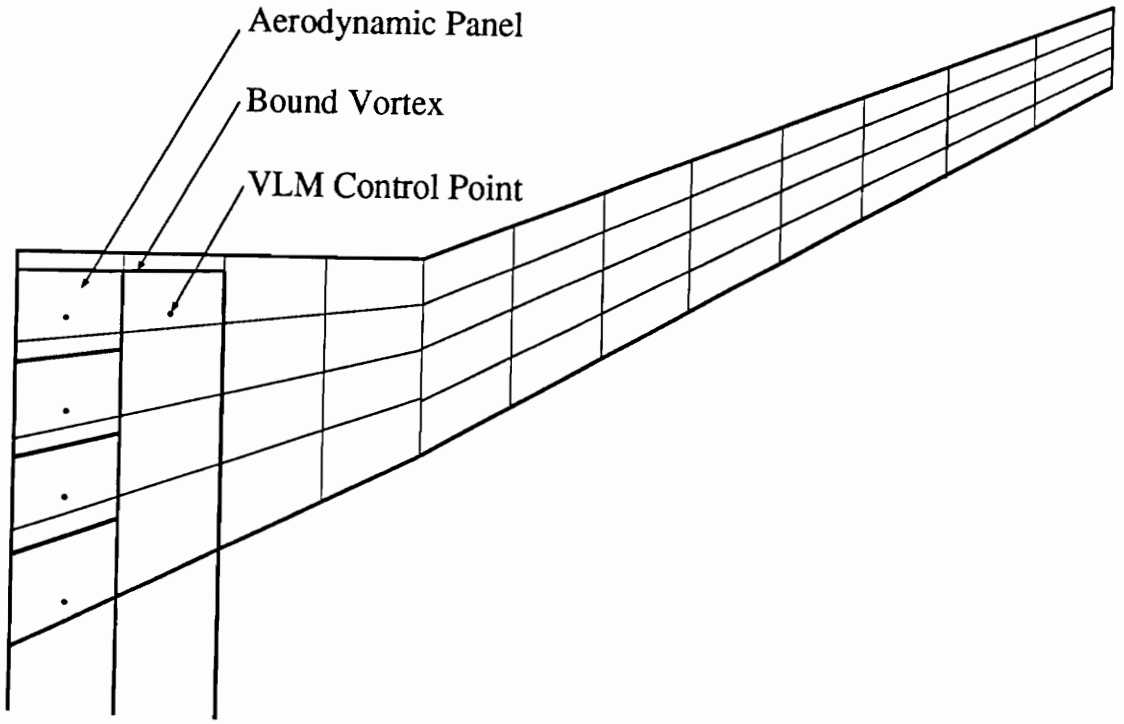

Figure 5.4. Sample wing with vortex-lattice panels

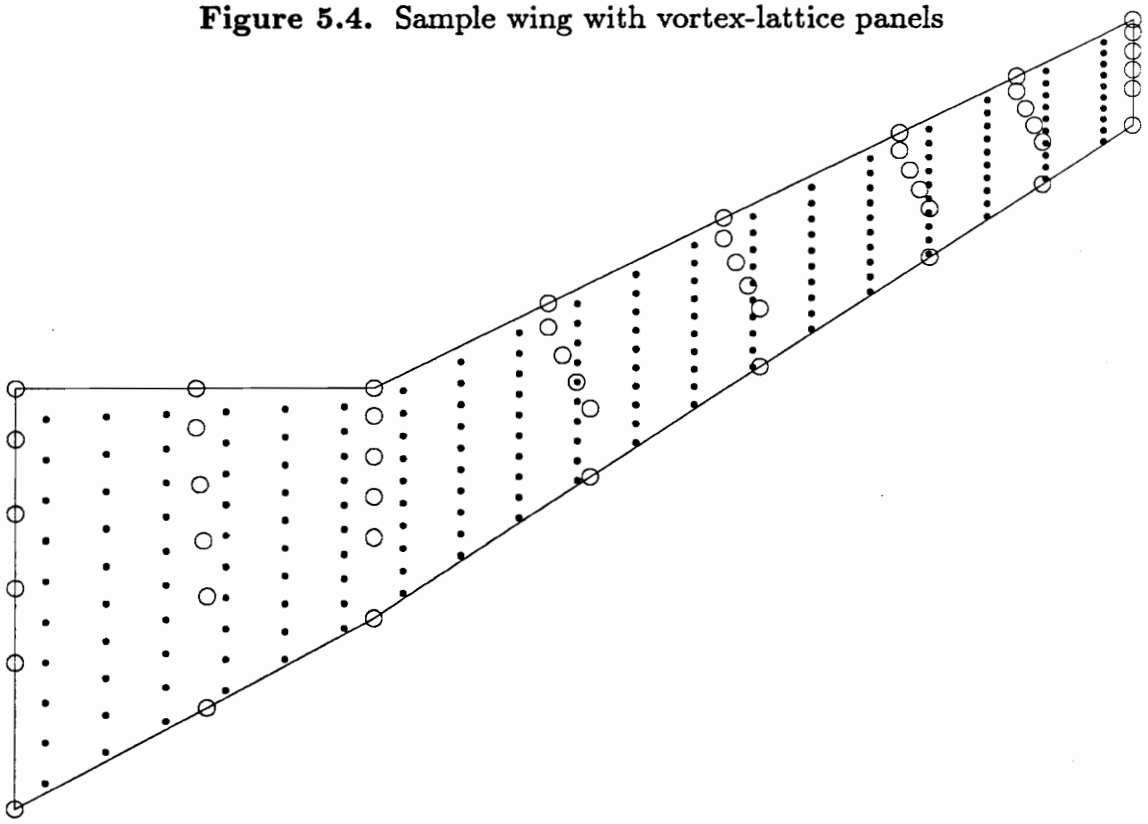

Figure 5.4. Sample wing with load set nodes and vortex-lattice control points

The interpolation of forces and deflections was accomplished with the use of an aerodynamic-structural interface. This interface provided the means to transfer forces acting on the aerodynamic panels to the load-set nodes and to transfer elastic deflections from the load-set nodes to the aerodynamic panels. Linear isoparametric shape functions were used with the grid defined by the load set nodes to unambiguously define aerodynamic points and interpolate deflections to the aerodynamic nodes or forces to the load set thus conserving work and energy (see appendix A.). With this type of interpolation, a deflection at the *ith* node only effects the wing locally near that given node.

5.3. Solution Procedure

The coupled aerodynamic and structural system for this case was solved with a single Newton iteration, which was found to provide accurate results without prohibitive cost. As an initial guess for the single iteration, a rigid-wing approximation, $F^0_{aG} = \Phi^T F_{ar}$, $\alpha^0 = \alpha_r$, $\theta^0 = 0$, was used, where

$$F^0_{aG} = f_1(p,0,0) + q\alpha_r R\,, \tag{5.3}$$

$$\alpha_r = \frac{nW - \hat{N}^T f_1(p,0,0)}{q\hat{N}^T R}\,. \tag{5.4}$$

5.4. Drag Evaluation and Sensitivity

The induced drag was calculated in the *far-field* or *Trefftz* plane. In the far field, the negligible streamwise-flow variation yields a two-dimensional, cross-plane flow induced by the trailing vortex sheet. The circulation distribution across the wing can be represented by a Fourier series, [29], as

$$\Gamma(\psi) = 2bU_\infty \sum_{n=1}^{\infty} A_n \sin n\psi\,, \tag{5.5}$$

where b is the span and $\cos\psi = 2y/b$. Using the circulation distribution determined from the vortex-lattice method, the coefficients A_n can be found using a Fourier transform. Then the induced drag is calculated as

$$D_i = -\rho_\infty U_\infty^2 b^2 \sum_{n=1}^{\infty} n A_n^2 \sin^2 n\psi \,, \tag{5.6}$$

which may be then integrated to yield

$$C_{D_i} = \frac{C_L^2}{\pi AR} \left[1 + \sum_{n=2}^{\infty} n \left(\frac{A_n}{A_1} \right)^2 \right] . \tag{5.7}$$

The lift coefficient is determined from the total lift, $C_L = L/qS$, with the lift force obtained by an integration of the lift per unit span as $L = \int l\, dy$ and $l = \rho_\infty U_\infty \Gamma$. The computations were performed with 32 terms in the series.

The viscous drag on the wing is obtained by first determining the local section drag in the streamwise direction, C_{d_v}, from the airfoil drag polar given in [26]. The total viscous drag, C_{D_v}, can then be determined by integrating the section drags over the span of the wing.

The remaining drag is associated with the fuselage and tail, $C_{D_{ft}}$. Since the aerodynamic shape of these surfaces is not being designed in this example, their contribution is assumed constant. This constant was determined as

$$C_{D_{ft}} = C_{D_{a/c_0}} - C_{D_{w_0}} \,, \tag{5.8}$$

where $C_{D_{a/c_0}}$ is the drag coefficient of the reference aircraft at zero angle of attack, and $C_{D_{w_0}}$ is the drag coefficient of the initial design wing at the same angle of attack. While this above approximation is very crude, a detailed analysis of the fuselage and tail is beyond the scope of this study.

The drag sensitivity for the flexible wing may be determined by first recognizing that the drag is a function of the design parameters, the angle of attack, and the wing deformation. Functionally this is given as

$$D = D(p, \alpha, \theta)\,. \tag{5.9}$$

The sensitivity can then be determined with the chain rule as

$$D' = \left(\frac{\partial D}{\partial p}\right)_{\alpha,\theta} + \left(\frac{\partial D}{\partial \alpha}\right)_{p,\theta} \alpha' + \left(\frac{\partial D}{\partial \theta}\right)_{p,\alpha} \theta'\,, \tag{5.10}$$

where the subscripts denote the variables held constant. Note that α' and θ' found in Eq. (5.10) are determined from the system presented in the previous section, and the partial derivative of the drag terms are calculated from forward differences. Equation (5.10) often includes large terms of opposite signs that cancel one another. Because of this property the accuracy of D' is often poor. Improvements to these calculations in [30] have limited errors to under 10% which was considered sufficient.

5.5. Approximate Optimization Procedure

The wing optimization was formulated as a sequential approximate optimization algorithm with move limits. Each approximate optimization problem starting from an initial design p^0 is formulated as:

$$\textit{minimize} \quad W(p) = W(p^0) + \sum_i^{n_p} \frac{\partial W}{\partial p_i} \Delta p_i \tag{5.11}$$

$$\begin{aligned} \textit{such that} \quad & g_s(p^0) + \sum_i^{n_p} \frac{\partial g_s}{\partial p_i} \Delta p_i \geq 0, \\ & V(p) \geq V_r, \\ & L_s(p, W) \leq L_{s_r}, \\ & R_c(p, D) \geq R_r, \\ \textit{where} \quad & D = D(p^0) + \sum_i^{n_p} \frac{\partial D}{\partial p_i} \Delta p_i, \end{aligned}$$

and where the vector g_s represents the structural constraints on the stresses, strains and aeroelastic stability and n_p is the number of design variables. The quantities V and V_r are the available wing volume and the required fuel volume, respectively. The quantities L_s and L_{s_r} are the landing speed and the required landing speed, respectively. The calculated range, R_c, depends upon the total drag of the aircraft and is required to be greater than the range of the reference aircraft. The range constraint is calculated using the exact range relationships with a linear approximation to the drag.

The optimizer used is the NEWSUMT-A program [31], which is based on an extended interior penalty function procedure, and allows for various levels of constraint and objective function approximations.

5.6. Optimization Results

The optimization process was begun from a nominal design without regard to the initial quality. The design problem required approximately 57 cycles to converge, with each iteration cycle taking approximately 1100 CPU seconds on an IBM 3090. The initial and final designs are tabulated in Table 5.4 and the initial and final planforms are sketched in Fig. 5.5. We see that the final wing configuration is dramatically different from the initial design and that of the reference aircraft. The final design has a relatively low aspect ratio of 10.61 and a span of 38.8 meters; (double the total distance from the root to the tip in Table 5.4 to obtain the total span for the aircraft). Additionally, the root chord is very large, 8.8 meters, giving the design a delta-wing appearance. The combination of this delta-type wing in conjunction with the tip extension provided a wing with low bending moments at the root to minimize the necessary structural weight.

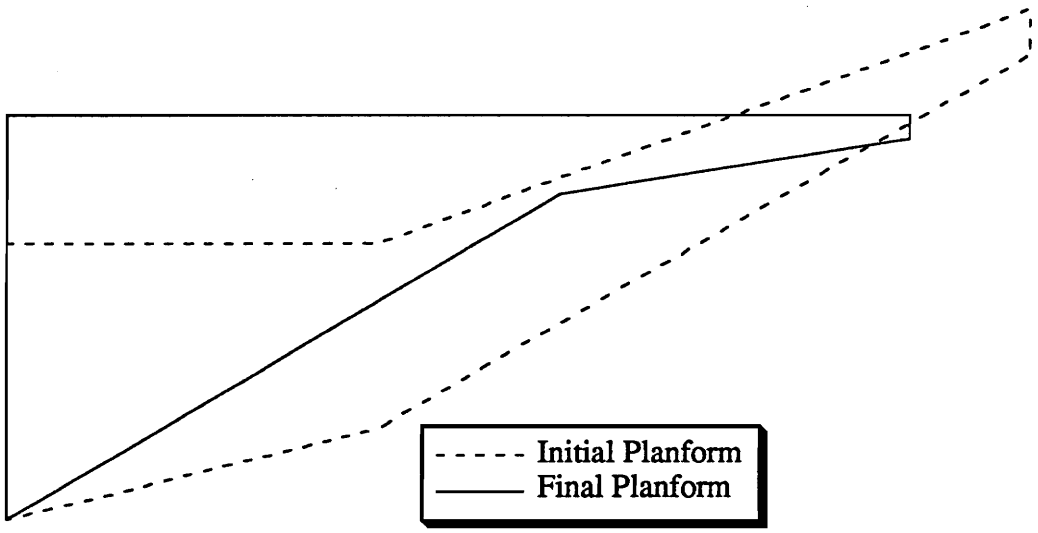

Figure 5.5. Initial and Final Wing Planforms – Initial Combined Design,Subsonic Transport

Of interest is how the design wing differs from the that of the reference aircraft. With so much of the wing loading for the design wing near the root, its structural weight is considerablely lower than that of the reference aircraft. While the dramatic difference between the two weights may be more pronounced than is realistic, it is clear that the design wing offers distinct weight advantages over a more conventional design. The penalty for this light, delta-type wing is in fuel costs. The design wing uses 32% more fuel than the reference aircraft. This difference can be attributed to the fact that the reference aircraft flies at a more efficient Mach number, and has better aerodynamic efficiency. However, this increase in fuel weight was more than offset by the structural-weight savings; (recall that no accounting for fuel economy is made in the objective function).

It is instructive to consider the iteration history of the design optimization. In Fig. 5.6, the convergence history of the gross weight is presented. The initial decrease followed by an increase in the weight resulted from the omission of a landing-speed constraint at the beginning of the optimization. When it became

Table 5.4. Initial and Final Designs for Subsonic Transport Wing

	Initial Design*	Final Design
Gross Weight (N)	501,100	444,600
Total Wing Weight (N)	60,290	18,490
Usable Fuel Weight (N)	40,000	36,020
Range Margin	0.9%	0.0%
Chord Lengths (m)		
Root	6.000	8.800
Break	4.000	1.727
Tip	1.000	0.523
Distance from Root to Break (m)	8.000	11.900
Distance from Break to Tip (m)	14.000	7.523
Total Wing Area (m^2)	150.0	142.19
Aspect Ratio	12.91	10.61
Leading Edge Sweep Angle (deg)	-20.05	0.0
Ply Orientation (deg)	26.1	21.3

* Some constraints violated

apparent that the wing was shrinking to the point that the aircraft could not land at a high-altitude airport, a landing-speed constraint was gradually introduced. Consequently, the wing area increased to allow for such landings with an attendant weight increase. However, once this constraint was satisfied, the wing area changed only slightly and the weight decreased again with more efficient planforms and structural thicknesses. The landing-speed constraint was active at all times, and effectively imposed a lower bound on the wing area for a given gross weight.

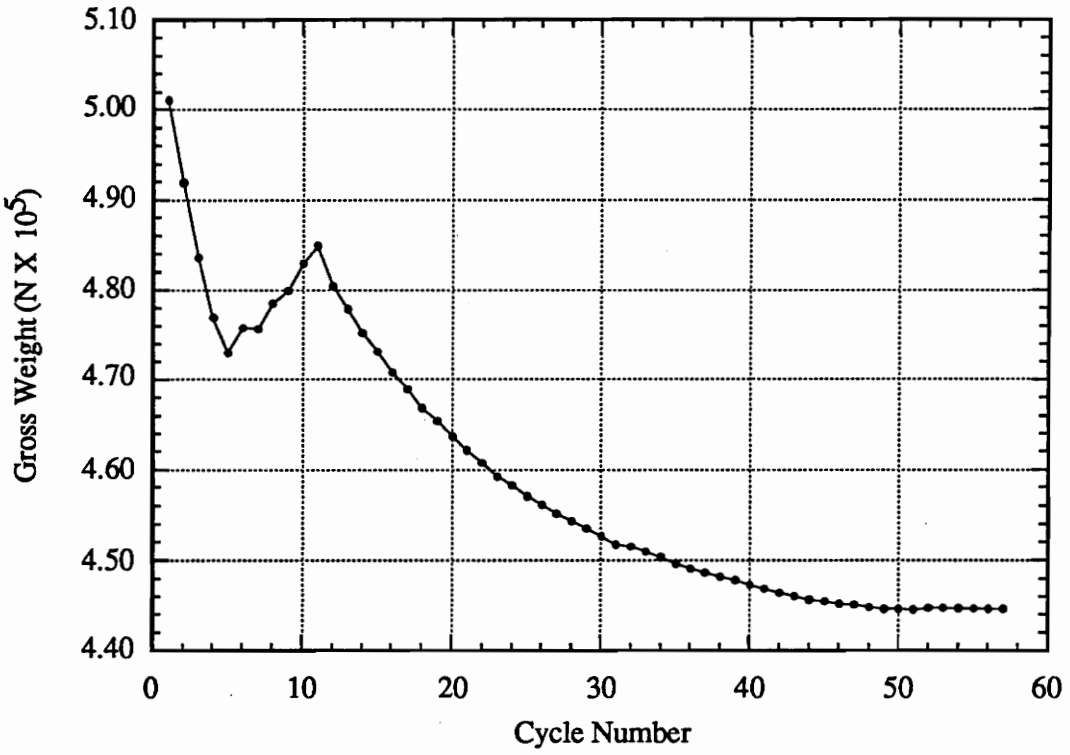

Figure 5.6. Weight History – Initial Combined Design, Subsonic Transport

The iteration history of the wing aspect ratio is shown in Fig. 5.7. An inspection of this figure reveals the inefficiency of the optimization, which first increased the aspect ratio, and then lowered it. This inefficient convergence is partly due to surplus structural material in the initial design and to the poor initial guess of the planform.

As expected the subcritical Mach number of 0.68 did not require any sweep and the optimization completely removed the sweep of the outboard-section leading edge, as illustrated in the planform design in Fig. 5.5. The iteration history of the leading-edge sweep angle in shown in Fig. 5.8. Due to the way the design variables have been selected, there was necessarily some forward sweep of the quarter chord.

Other important lessons were learned from the convergence studies. It was found that tight move limits on the order of 4–6% were needed for the approximate

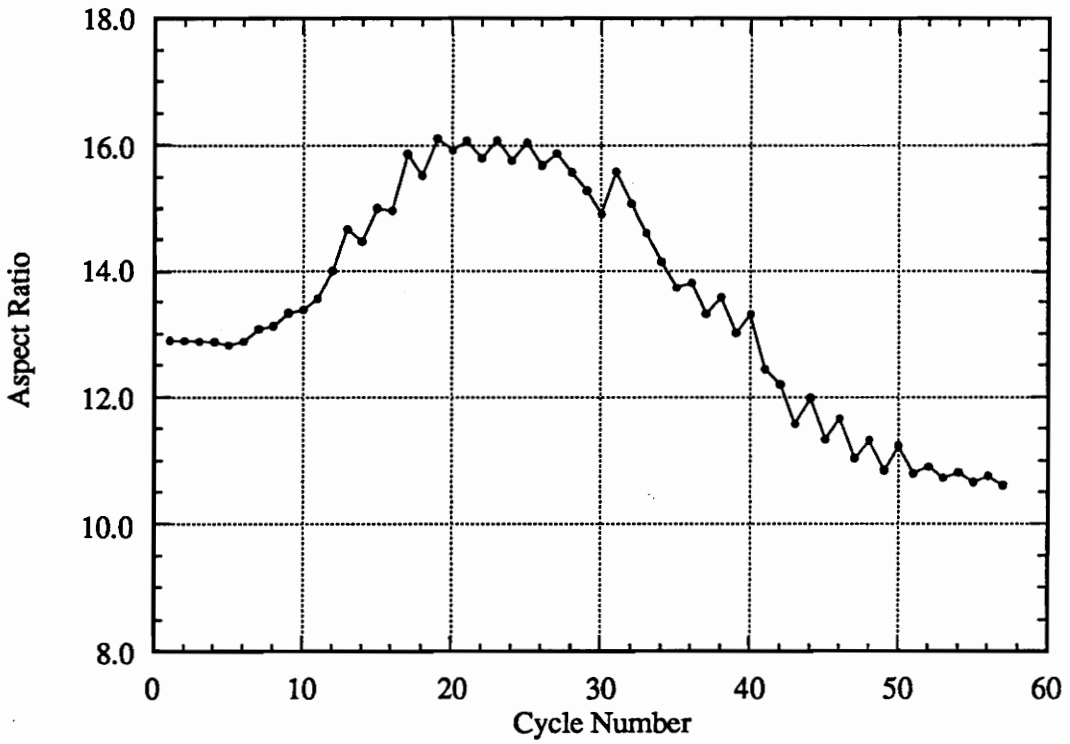

Figure 5.7. Aspect Ratio History – Initial Combined Design, Subsonic Transport

optimization cycle (except at the last four cycles where the move limits were reduced to 2%). The jaggedness of the convergence history of the aspect ratio, Fig. 5.7, indicates that move limits could not be increased. Tighter move limits would result in smoother but slower convergence. Also, convergence required a nearly feasible initial design with only small constraint violations. Since the number of optimization cycles required for convergence was large, we believed that a better initial design would reduce CPU costs. Such an initial design could be generated by using a less complex structural model. This approach is a form of variable-complexity modeling and is discussed below.

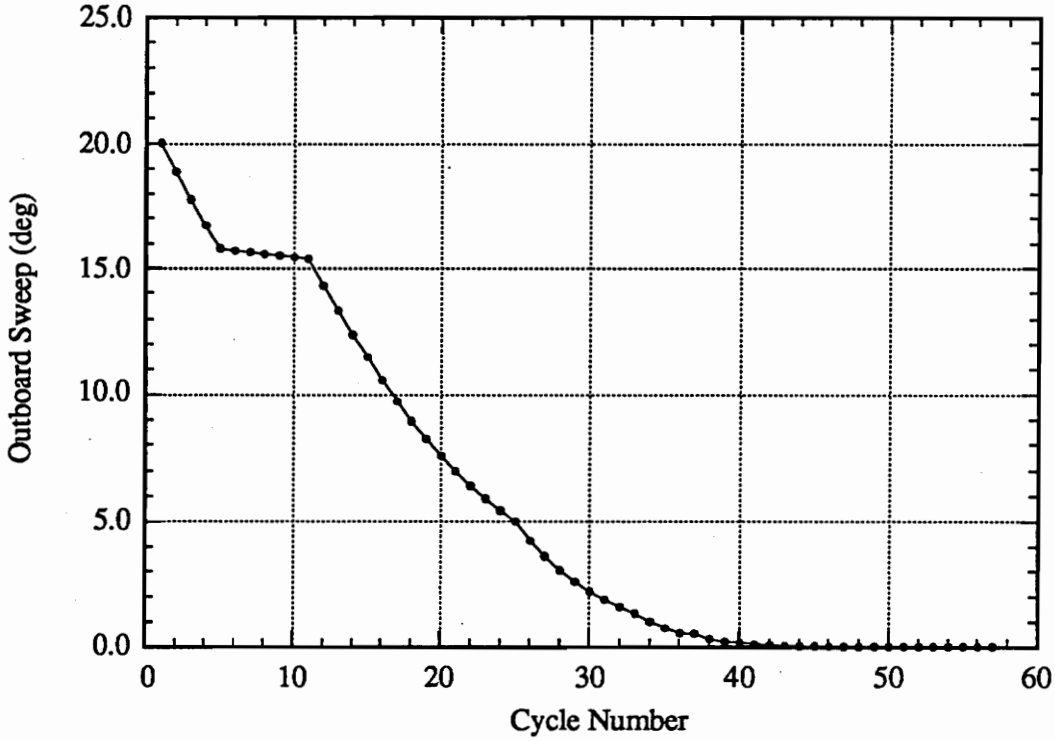

Figure 5.8. Outboard Leading Edge Sweep History – Initial Combined Design, Subsonic Transport

5.7. Aerodynamic design with algebraic weight equation

Since the number of iterations and required CPU time mentioned above are quite large it seems logical that one could reduce them with a better initial design. This initial design can be provided by the use of variable-complexity modeling as discussed previously in chapter 4. For this case the simpler problem of aerodynamic design with wing weight estimated by an algebraic weight equation taken from the conceptual design code FLOPS [32], was solved. These weight estimation routines rely on correlations developed using wing weights of actual aircraft, as well as structural optimization studies with the TSO program, [33].

The calculation of the vertical loads for this problem is exactly the same as that of the previous example, while the calculation of the vertical displacements is replaced by algebraic weight relations that approximately account for the effects

of geometry on wing weight. The solution to the coupled system of equations is trivial. The resulting solution is merely the rigid-wing condition given by

$$F_{aG} = f_1(p,0) + q\alpha_r R, \tag{5.12}$$

$$\alpha_r = \frac{\frac{1}{2}nW - N^T f_1(p,0)}{qN^T R}. \tag{5.13}$$

These relations are very inexpensive as the generalized aerodynamic influence matrix, qA, and the generalized flexibility matrix, S_G, are unnecessary.

For the sensitivity derivatives of the rigid wing we differentiate Eqs. (2.5) and (2.8) (ignoring θ) with respect to p to obtain

$$JY' = f', \tag{5.14}$$

with

$$Y' = [\, F_a' \quad \alpha' \,]^T, \tag{5.15}$$

and

$$f' = [\, f_1' \quad f_2' \,]^T, \tag{5.16}$$

and the Jacobian as

$$J = \begin{bmatrix} I & -\partial f_1/\partial\alpha \\ -\partial f_2/\partial F_a & 0 \end{bmatrix} = \begin{bmatrix} I & -qR \\ N^T & 0 \end{bmatrix}. \tag{5.17}$$

Note that the Jacobian for this problem contains no terms which are computationally expensive so we again have substantial computational saving over the complex model.

The design formulation and optimization procedures for the simple-model problem is almost exactly the same as that of the previous example, except that the

structural constraints and design variables are unnecessary. The reduced set of design variables consist of the six planform variables, the two twist variables, and the performance variables. Note that the twist variables for this analysis represent the shape of the wing during cruise, and do not define a *jig shape* as with the flexible wing design.

In the optimization, it was not necessary to linearize the weight relations as the cost of the calculation was minimal. Typically the weight predicted by the simple-model analysis was much larger than the weight obtained from the complex model. Part of the difference is due to the high allowables corresponding to future advance materials used here and not included in the wing weight correlations. Another contribution to the difference is that the flexible analysis does not include all the load cases on the wing and all the constraints (such as buckling).

5.8. Aerodynamic design optimization results

The optimization results from the aerodynamic design with algebraic weight equations described in section 5.7, is now considered. Two versions of the weight equations were considered. An unscaled one given by FLOPS (See Appendix B.), and a scaled weight that corresponds to the advanced material properties and the same load conditions and structural constraints as in the detailed finite-element model was used in the combined optimization. The scaling factor was chosen so that the gross weight of the simple-model and the detailed finite-element analysis would match for one planform. The planform selected for this was the final design of the combined problem described previously. With this planform the scaling factor was found to be 0.4, which represents a drastic weight difference.

The aerodynamic design problem was begun using the unscaled algebraic weight equations starting with the same initial planform as that of the combined design

problem (see Fig. 5.5). The initial and final designs are presented in Table 5.5 with a sketch of the two planforms given in Fig. 5.9. The aerodynamic optimum obtained with the unscaled weight equation is considerably different than that obtained from the combined problem. Because of the higher weight of the structure, the design goes farther in the direction of sacrificing aerodynamic efficiency for improving structural efficiency. The result is a very low aspect ratio of 6.32. The unscaled aerodynamic design optimum also uses more fuel than the complex-model design (38.0kN vs. 36.0kN). Figures 5.10 and 5.11 give the iteration history of gross weight and aspect ratio of the simple model with each cycle using approximately 100 CPU seconds on an IBM 3090 which is less than 10% of the complex-model design CPU time.

The aerodynamic design problem was repeated using the scaled-down weight equations once again starting with the same initial design as that of the initial combined design problem. The initial and final designs are presented in Table 5.5 with a sketch of the two planforms given in Fig. 5.12. The aerodynamic optimum obtained with the scaled weight equation closely approximates the planform for the combined aerodynamic-structural design optimum. This is an encouraging result since the goal of the aerodynamic design is an improved initial design point. Additionally, the final weight of the wing is much closer to that of the combined design. Figures 5.10 and 5.11 also give the iteration history of gross weight and aspect ratio of the scaled aerodynamic optimization.

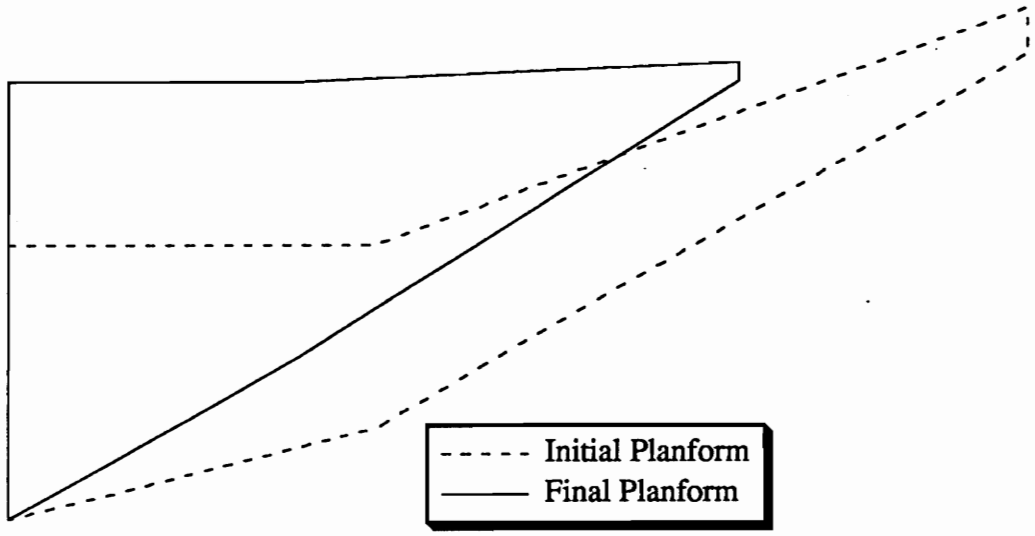

Figure 5.9. Initial and Final Planforms – Unscaled Aerodynamic Design, Subsonic Transport

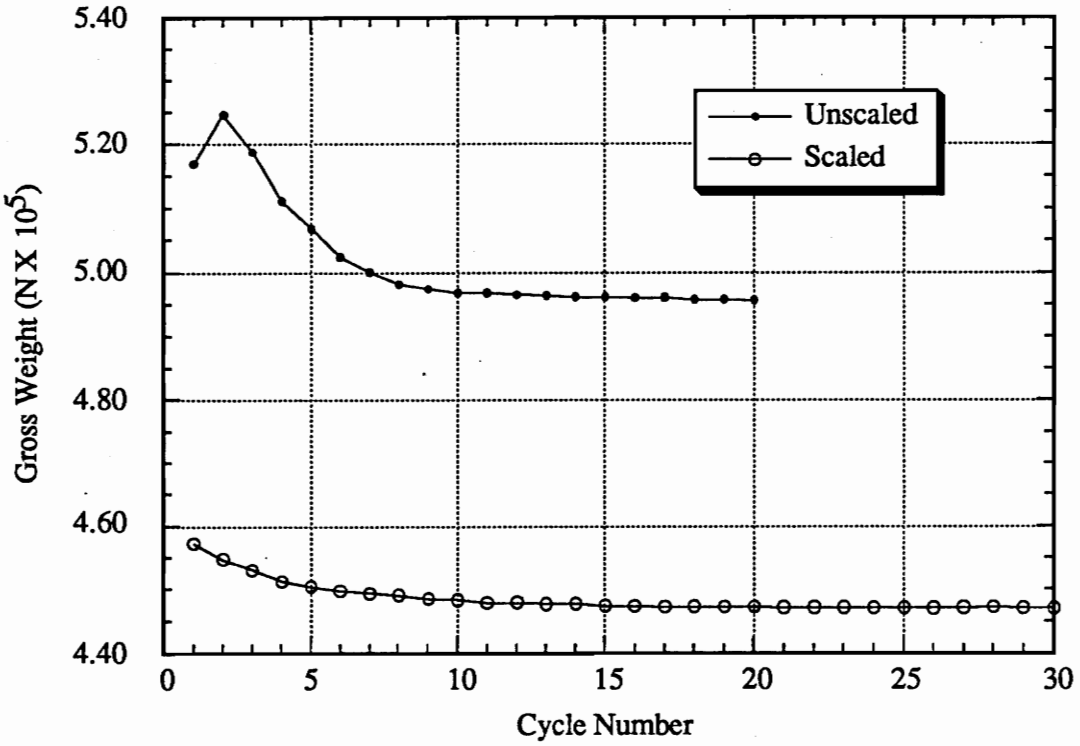

Figure 5.10. Weight History – Aerodynamic Design, Subsonic Transport

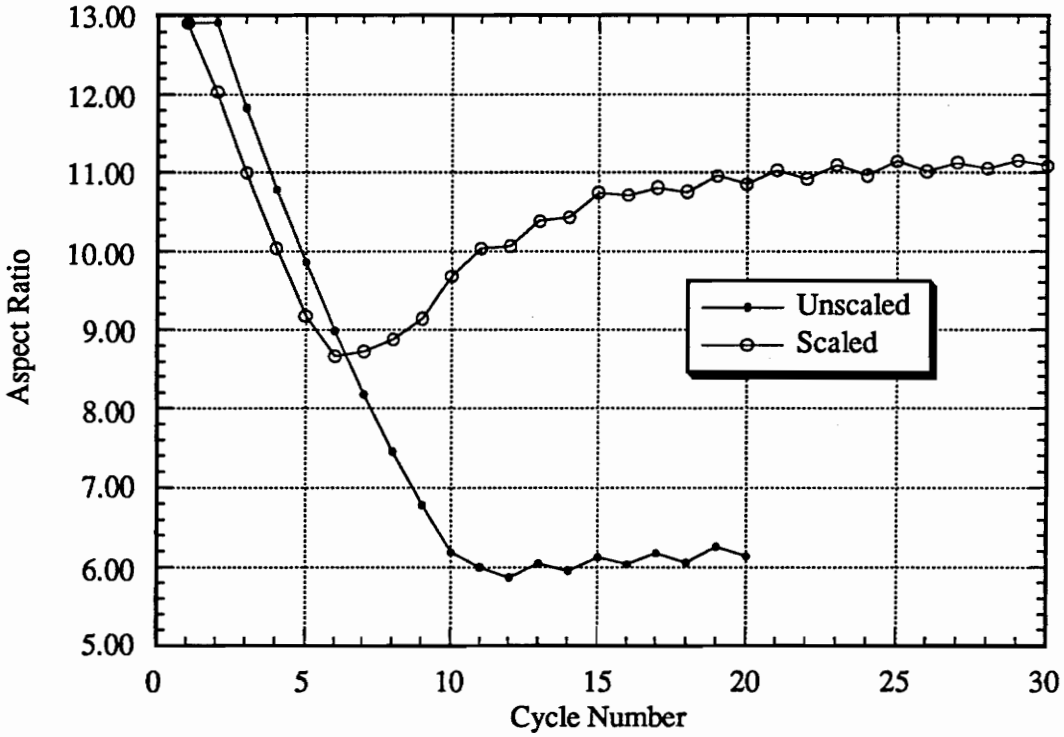

Figure 5.11. Aspect Ratio History – Aerodynamic Design, Subsonic Transport

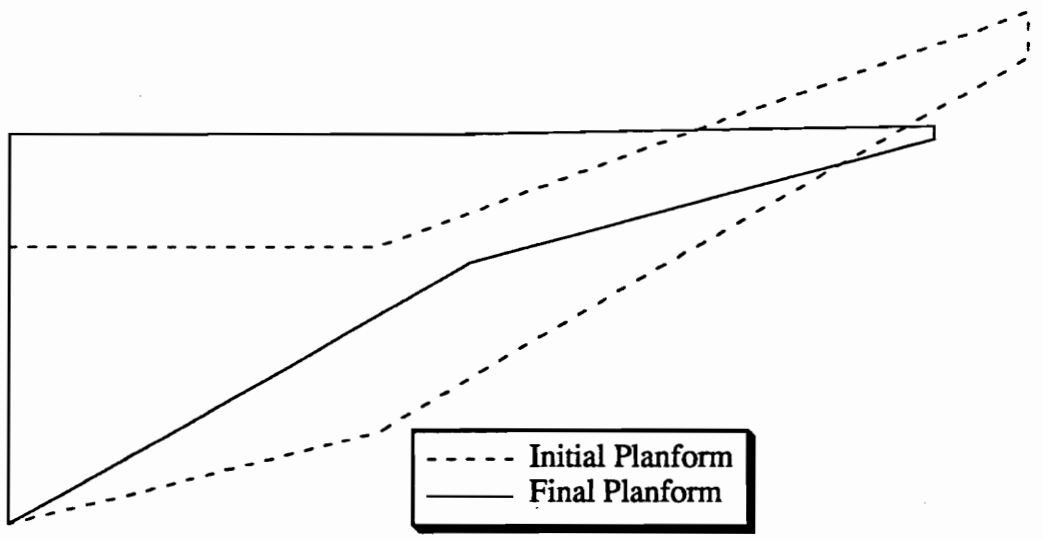

Figure 5.12. Initial and Final Planforms – Scaled Aerodynamic Design, Subsonic Transport

Table 5.5. Initial and Final Designs for the Aerodynamic Design Problem, Subsonic Transport

	Initial Design* Unscaled/Scaled	Optimum Design Unscaled	Optimum Design Scaled
Gross Weight (N $\times$ 10^5)	5.169/4.573	4.957	4.470
Total Wing Weight (N $\times$ 10^4)	7.234/2.649	5.758	2.043
Usable Fuel Weight (N $\times$ 10^4)	4.000	3.800	3.778
Range Margin	-6.67%/1.71%	0.0%	0.0%
Chord Lengths (m)			
Root	6.000	9.525	8.434
Break	4.000	5.990	2.784
Tip	1.000	0.396	0.294
Distance from Root to Break (m)	8.000	6.286	10.005
Distance from Break to Tip (m)	14.000	9.540	10.000
Total Wing Area (m^2)	150.0	158.45	141.0
Aspect Ratio	12.91	6.32	11.19
Leading Edge Sweep Angle (deg)	-20.05	-2.44	-1.05

* Some constraints violated

5.9. Combined design from aerodynamic optimum

With these two simple-model optimums in hand, the complex-model design problem was rerun using these designs as initial conditions (Fig. 5.13 gives a flowchart of this optimization approach). First, the combined-model optimization was restarted from the unscaled aerodynamic optimum. Since the aerodynamic design analysis only yields a planform and performance variables, it was necessary to estimate the

structural design variables. The initial value for these structural variables was selected to be the optimum structure for the nominal combined-model design case. Alternatively, a relatively inexpensive structural optimization (for fixed aerodynamic design) may be used at this point to get an initial structural design. Such an optimization may be also used to determine a good weight scale factor.

Figure 5.14 gives the convergence history of the aircraft gross weight and Fig. 5.15 gives the convergence of the wing aspect ratio. Substantially fewer iterations were required for this design (34) as compared with the nominal design case even though this initial start was not very good (see the large changes in aspect ratio in Fig 5.15). Figure 5.16 presents the CPU times for the various runs and reveals a substantial reduction of run time for this case. This figure also demonstrates the minimal cost of the aerodynamic design problem. The improvements of this optimum over that of the nominal analysis can be seen in Table 5.6 where we see a gross weight reduction of 1000N (compare to Table 5.4) even though the final planform as seen in Fig. 5.17 is not very different than the nominal case. It was first suspected that the nominal and new designs represented two local minima, but investigation revealed that this was not the case. It is now believed that numerical errors in the calculation of the drag sensitivities prevent the nominal design from reaching this lighter design. In any event, the difference in gross weight between the two designs is only 0.25%.

The final optimization considered is a complex-model design with the initial design point coming from the scaled, simple-model optimum. The initial and final designs are given in Table 5.6 with a sketch of the planform given in Fig. 5.18. It is clear that this initial guess is excellent and only a minimal amount of optimization was required (Figure 5.15 reveals that the aspect ratio varied only slightly). The

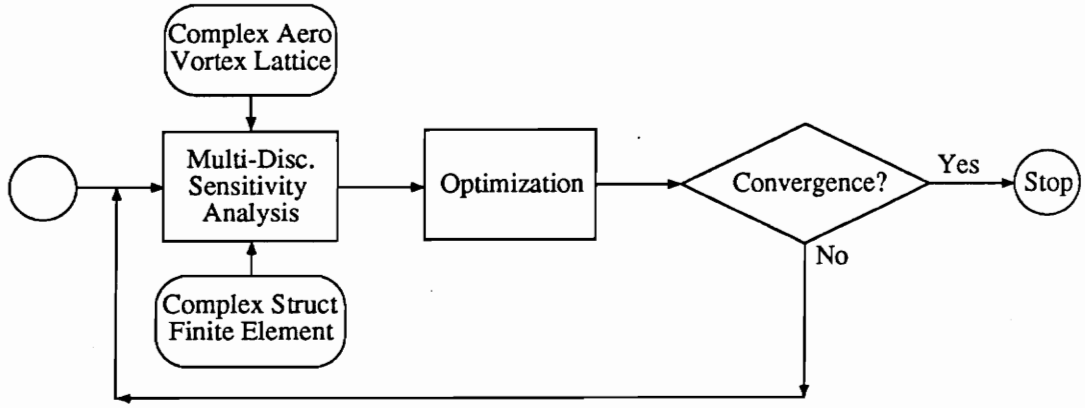

a) Single-Complexity Optimization

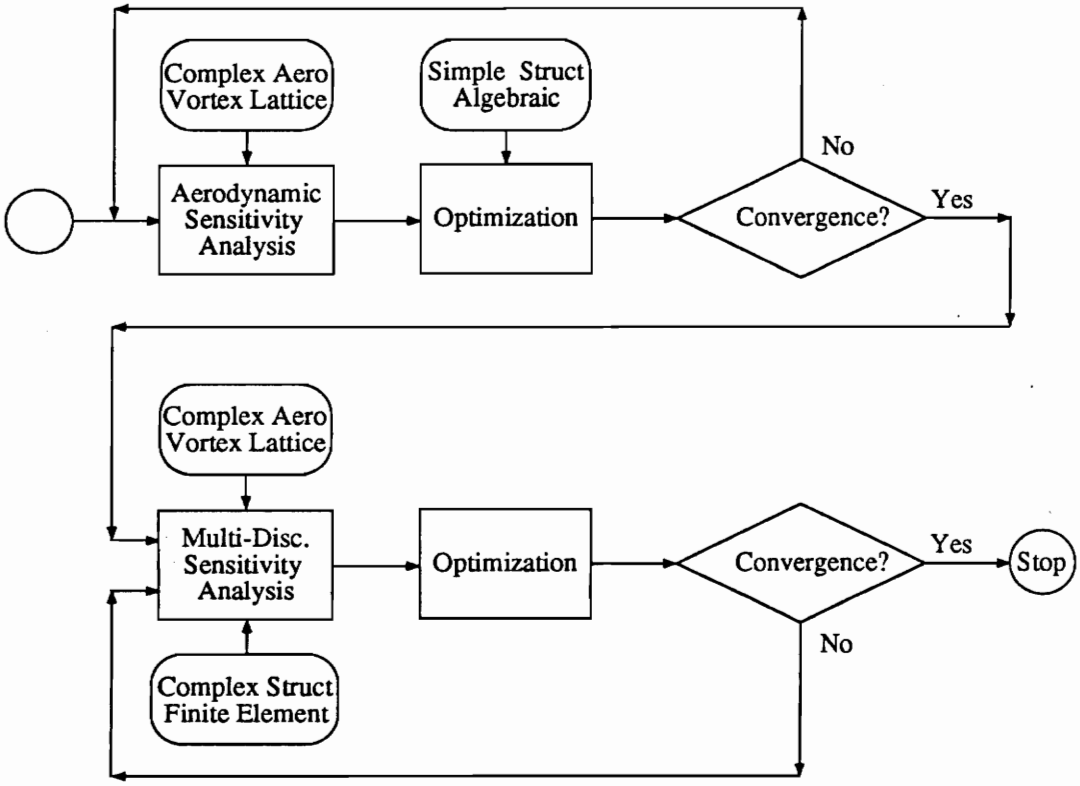

b) Variable-Complexity Optimization

Figure 5.13. Variable-Complexity Optimization Flowchart for Subsonic Transport

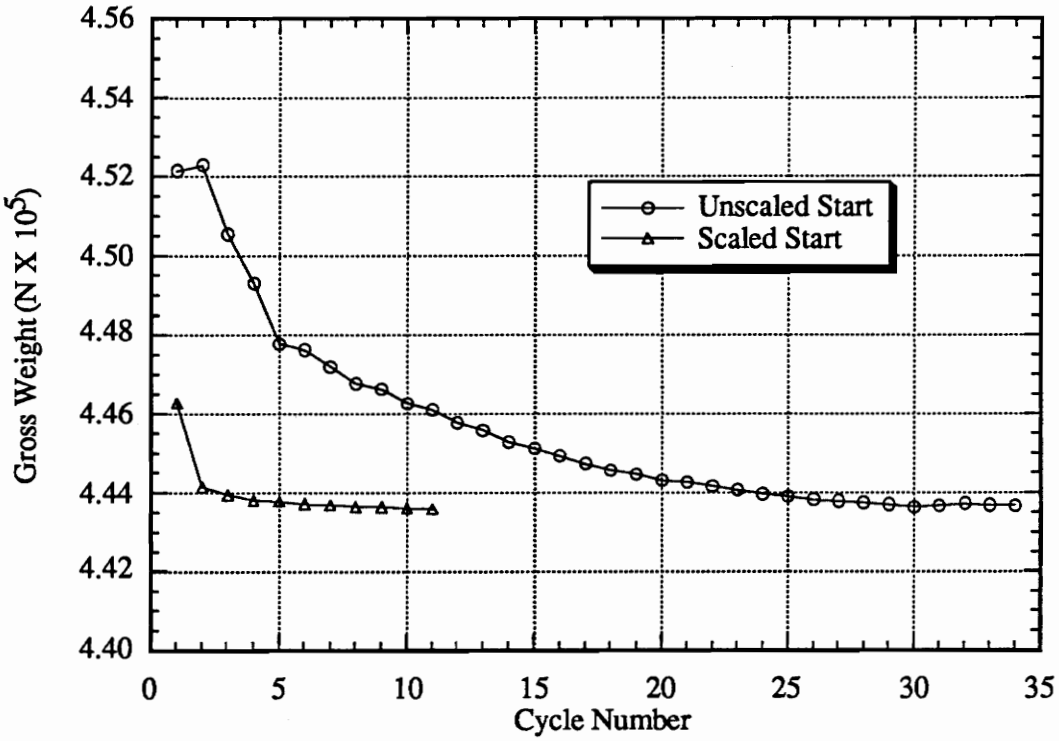

Figure 5.14. Weight History – Combined Design from Aerodynamic Final Design, Subsonic Transport

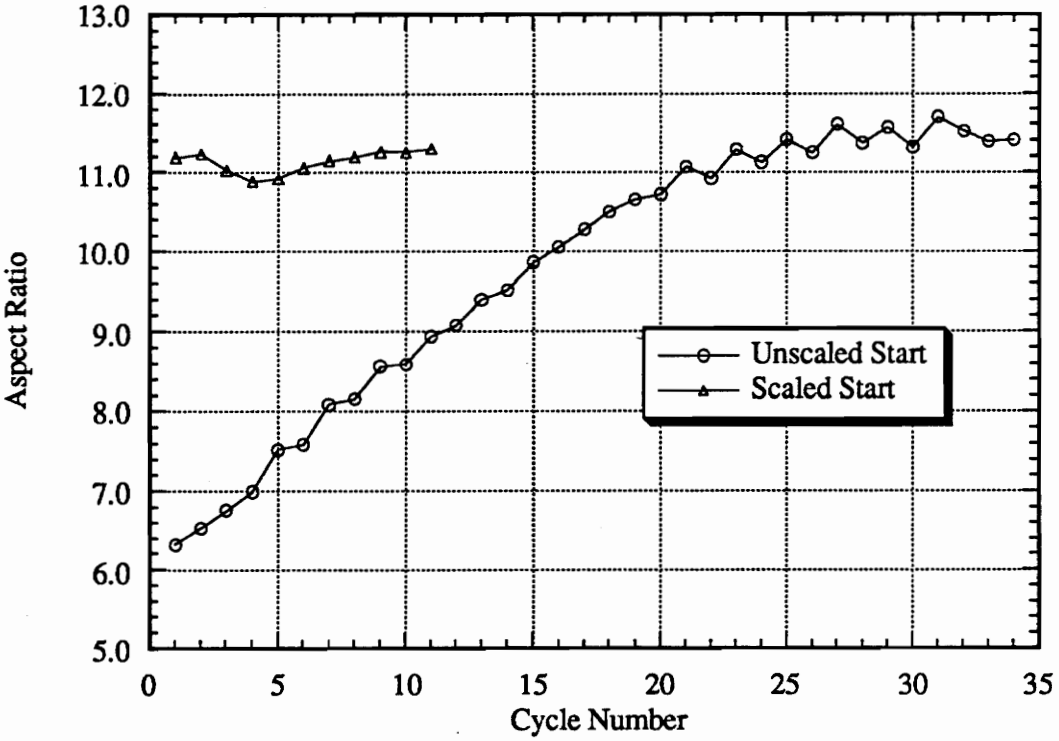

Figure 5.15. Aspect Ratio History – Combined Design from Aerodynamic Final Design, Subsonic Transport

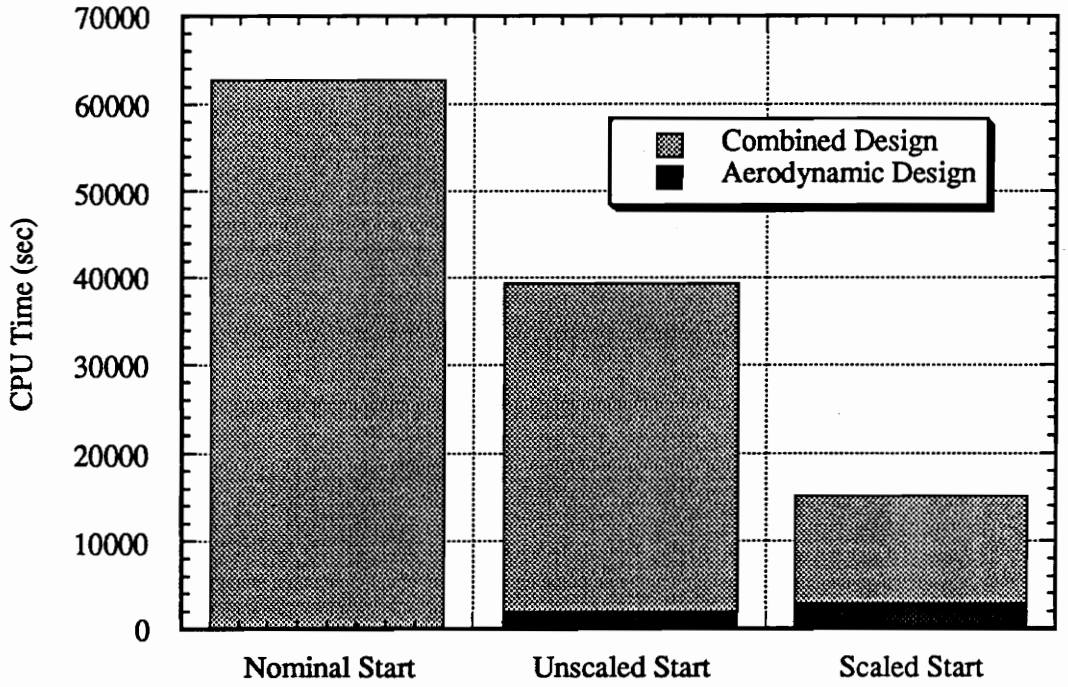

Figure 5.16. Computational Times for Variable-Complexity Strategies for Subsonic Transport

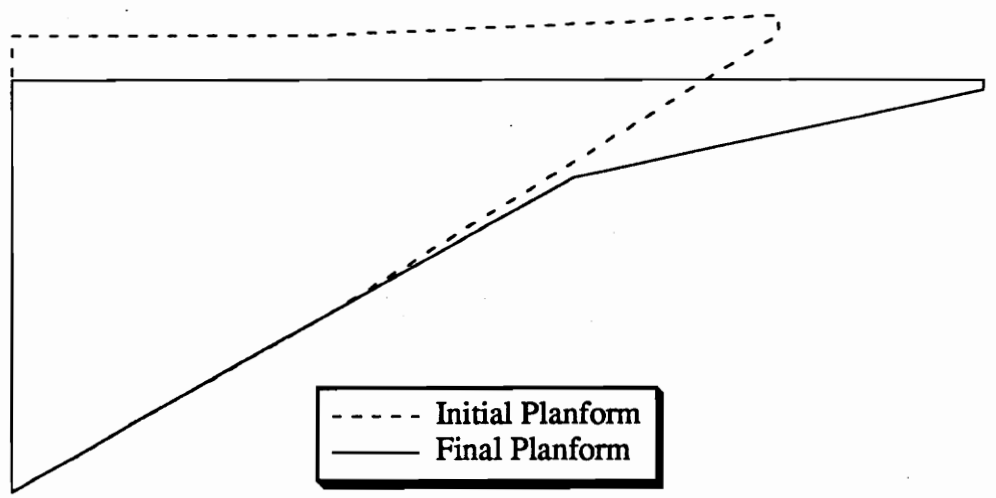

Figure 5.17. Initial and Final Planforms – Combined Design from Unscaled Aerodynamic Final Design, Subsonic Transport

convergence of the gross weight for this case is presented in Fig. 5.14 which demonstrates sufficient convergence in only 11 design cycles. Returning to Fig. 5.13 we see that this case uses only 25% of the CPU time necessary for the nominal design and it achieves a superior result. The optimum for this case is essentially the same as the optimum arrived at with the unscaled start (albeit with much less effort) which supports the quality of this procedure.

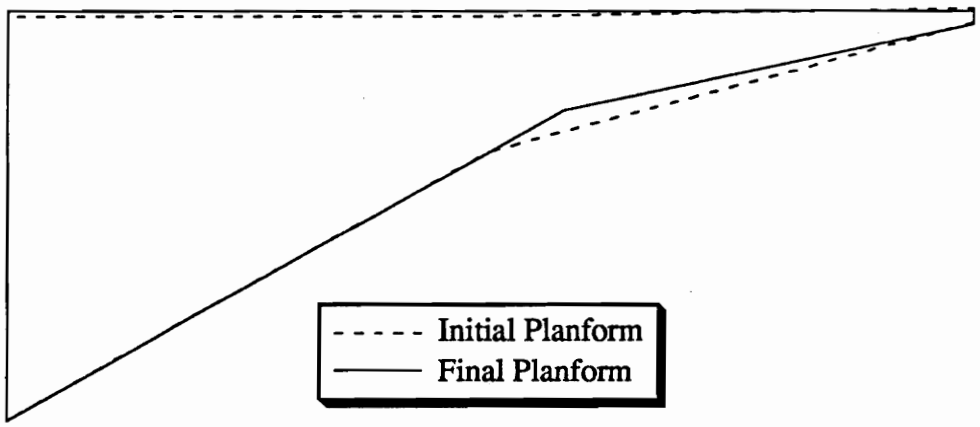

Figure 5.18. Initial and Final Planforms – Combined Design from Scaled Aerodynamic Final Design, Subsonic Transport

Table 5.6. Optimum for Combined Design from Aerodynamic Optima for the Subsonic Transport

	Unscaled Start	**Scaled Start**
Gross Weight (N)	443,600	443,600
Total Wing Weight (N)	19,500	19,510
Usable Fuel Weight (N)	35,530	35,440
Range Margin	0.0%	0.0%
Chord Lengths (m)		
Root	8.575	8.550
Break	2.031	2.061
Tip	0.198	0.266
Distance from Root to Break (m)	11.583	11.501
Distance from Break to Tip (m)	8.531	8.514
Total Wing Area (m^2)	141.88	141.85
Aspect Ratio	11.41	11.30
Leading Edge Sweep Angle (deg)	0.0	0.0
Ply Orientation (deg)	21.2	21.4

* Some constraints violated

6. DESIGN CASE 2: HIGH SPEED CIVIL TRANSPORT

For this case the aerodynamic design of a Mach 3.0 transport aircraft with a 6500 mi. range is considered. As with the subsonic design case, this problem was formulated to reduce the take-off gross weight while maintaining the given range. In this problem we consider only aerodynamic design using a simplified algebraic equation for the weights. This design can be considered a prelude to a combined aerodynamic-structural wing design using detailed structural models. The weights for the analysis are provided by a weight equation taken from FLOPS, as described for the subsonic aerodynamic design problem, see chapter 5. The baseline concept for this aircraft is provided by NASA's AST3I given in [34] (other examples of HSCT aircraft can be seen in [35] and [36]. Some specifications of the AST3I are given in Table 6.1 and a sketch of the vehicle appears in Fig. 6.1.

6.1. Supersonic transport design problem

An analytic wing definition was created to provide a practical representation of the complex wing geometry utilizing a minimum number of design variables, [37]. These variables are listed in Table 6.2 and consist of 11 planform variables, 7 airfoil variables, and 3 performance variables.

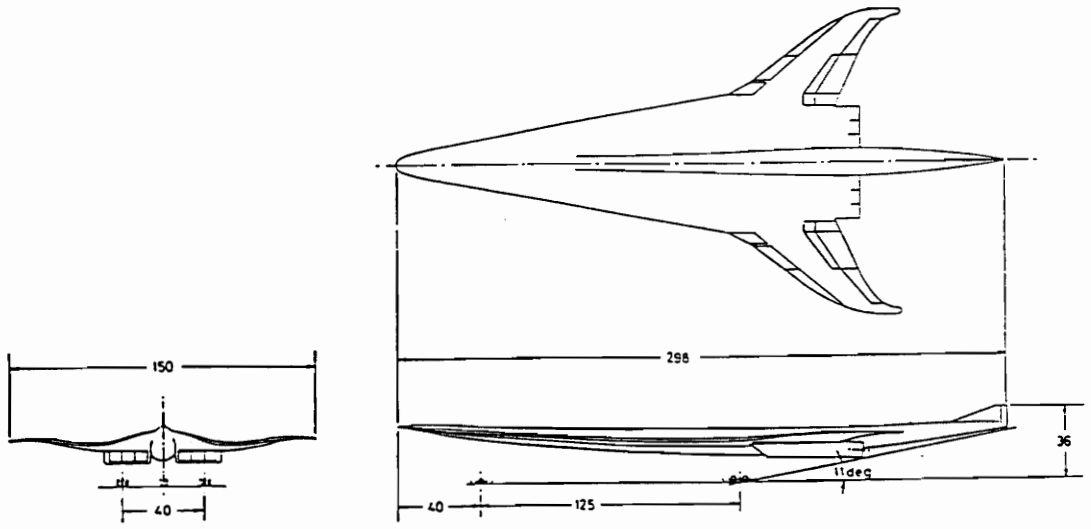

Figure 6.1. AST3I Configuration [34]

The first ten planform variables define the coordinates of break points for the leading and trailing edge. These break points define three straight line segments for the leading and trailing edges which are exponentially blended to provide a smooth transition between segments as in [38]. The final planform variable defines the wing semi-span as illustrated in Fig. 6.2.

The first four airfoil variables define a distribution of wing thickness across the span (see Fig. 6.3). These variables provide t/c at four wing stations and it is assumed that the actual wing thickness varies linearly between the points. The point of maximum thickness at each airfoil is assumed to be constant along the span and defined by the next design variable. Using the original AST3I aircraft as a basis, a provision for both supersonic and subsonic airfoil sections is maintained

Table 6.1. AST3I Specifications

Weights, lbs:		
	Wing	56,258
	Total structures	153,381
	Empty weight	263,658
	Operating weight	272,981
	Passenger weight(250)	41,250
	Passenger baggage weight	11,000
	Zero-fuel weight	327,796
	Mission fuel weight	385,900
	Gross weight	713,696
Wing:		
	Area, ft^2	12,185
	MAC, ft	129.65
	Span, ft	150.0
	Aspect ratio	1.85
	Root t/c (%)	2.0
	Tip t/c (%)	3.5

by the next two design variables. The first of these gives the leading-edge half angle for supersonic sections by defining the linear relation between the wing t/c and this angle. The final airfoil variable provides the leading-edge radius for the subsonic sections.

The first performance variable gives the flight fuel for the aircraft which is utilized for cruise and loiter. The final two design variables provide information for the cruise profile giving the starting altitude and the climb rate. This rate is assumed to be a constant until the aircraft reaches a maximum altitude of 70,000 ft. and levels off.

A total of 37 constraints have been employed in this design problem and are

Table 6.2. Design Variables for HSCT Wing [34]

11 Planform Design Variables	1. LE Break 1, x 2. LE Break 1, y 3. LE Break 2, x 4. LE Break 2, y 5. LE Wing tip, x 6. TE Break 1, x 7. TE Break 1, y 8. TE Break 2, x 9. TE Break 2, y 10. Tip chord 11. Wing semi-span
7 Airfoil Design Variables	12. t/c at wing root 13. t/c at LE break 1 14. t/c at LE break 2 15. t/c at tip 16. Max t/c location 17. "Slope" of leading edge half angle and t/c 18. Leading edge radius (subsonic sections)
3 Performance Design Variables	19. Flight fuel 20. Initial cruise altitude 21. Climb rate

listed in Table 6.3. The first set of these constraints prevents the optimizer from generating unrealistic designs. Specifically, the wing chords and thicknesses have set minimums of 7 ft and 1.5% (t/c) respectively. The wing breakpoint locations were forced to be arranged sequentially on the wing and to be less than the wing semi-span. Additionally, the root trailing-edge sweep angle was limited to positive values during one design case.

In a number of preliminary results, the optimizer was producing wings with

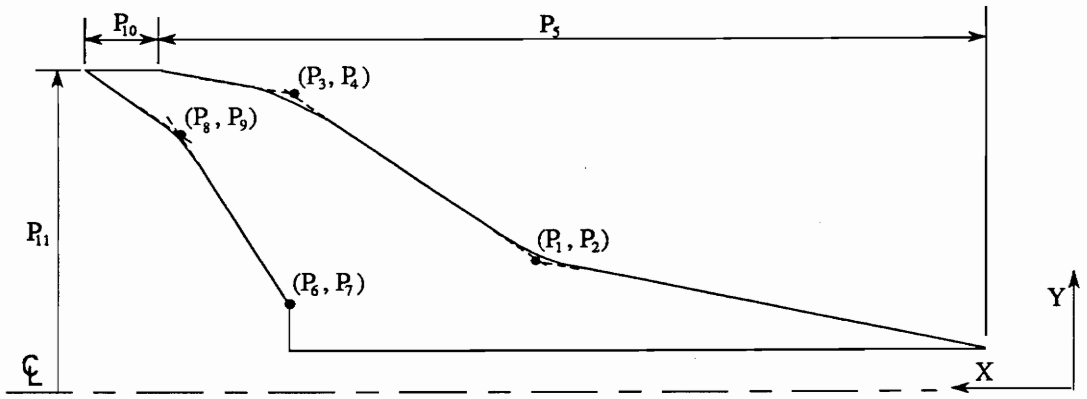

Figure 6.2. HSCT Planform Description Parameters

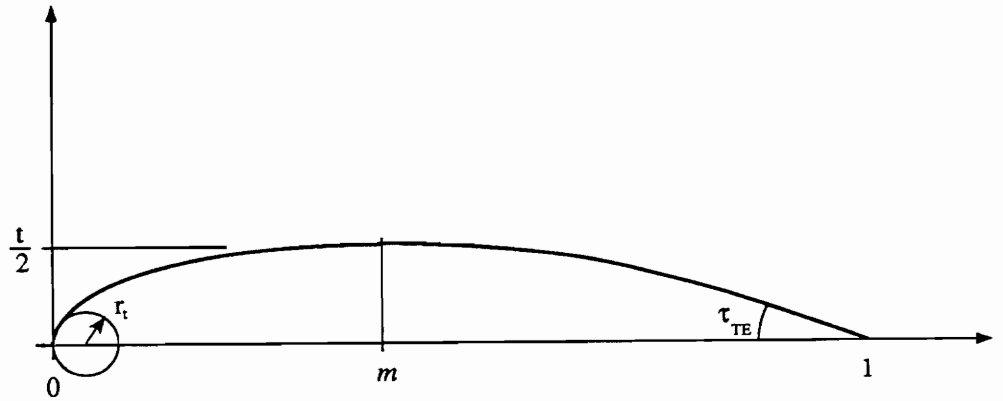

a) Round Leading Edge

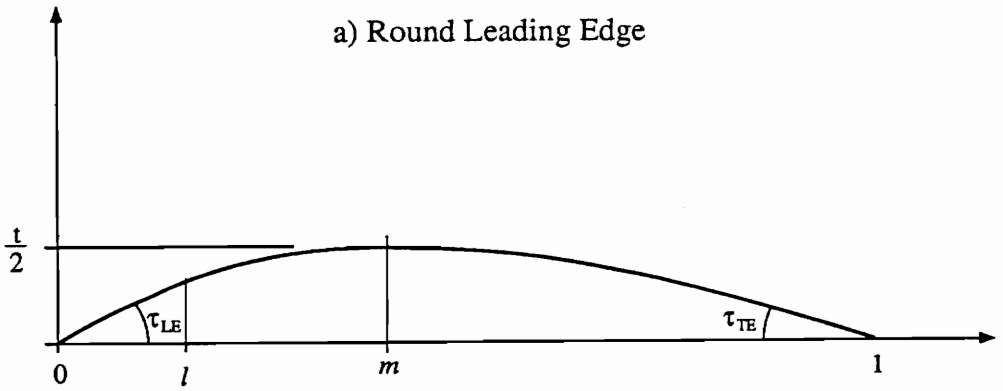

b) Sharp Leading Edge

Figure 6.3. Airfoil Description Parameters for HSCT Design

an highly swept region at the tip know as a "spike" (see Fig. 6.4). Investigations revealed that the optimization was taking advantage of small advantages in wave and drag due to lift. As these geometries were deemed unrealistic, a final geometric constraint of 3 ft was placed on the width of the wing *normal* to the leading edge.

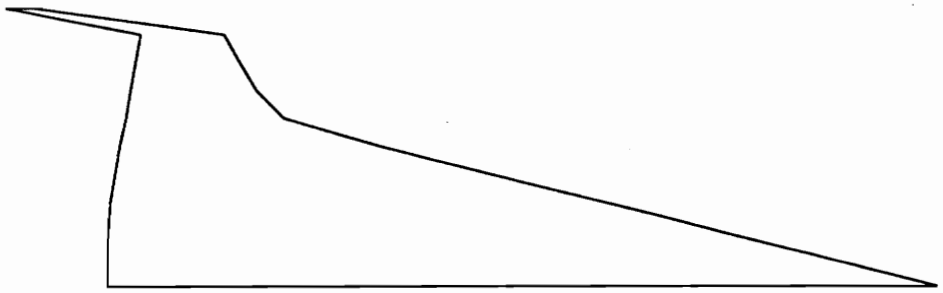

Figure 6.4. An Example of a "Spiked" Wing Planform

The next set of constraints place requirements on the performance of the aircraft in general. These constraints include a minimum range of 6500 miles. A maximum landing angle of 12° is imposed to prevent any difficulties with "tail-scrape". Landing performance considerations were also made by limiting the approach lift coefficient to less than 1.0 (145 kts at 5000 ft with 50% fuel load on a 90° F). The section lift coefficients at the same conditions were not allowed to exceed 2.0. It was assumed the mission fuel would be carried entirely in the wing and therefore the wing was required to have sufficient volume to hold this fuel (it was assumed that only 50% of the wing's volume is available for fuel storage). The final performance constraint limited the aircraft's maximum altitude to 70,000 ft for cabin depressurization safety considerations.

Table 6.3. Design Constraints for HSCT Wing

21 Geometric Constraints	1.–11. Wing chords
	12.–15. Wing thicknesses
	16.–19. Break point locations
	20. Root TE angle
	21. "Spike" prevention
16 Performance Constraints	22. Range
	23. Landing α
	24. Fuel volume
	25. Landing C_L
	26.–36. Landing section C_l
	37. Maximum altitude

6.2. Supersonic aerodynamic analysis

As in the previous design case, drag provides the major aerodynamic consideration for the design. The drag consists of the volumetric wave drag, the drag due to lift, and the friction drag. Evaluation of these terms represents a considerable cost increase over drag evaluation for the subsonic design case (for a similar level of accuracy). This is the motivation for the use of variable-complexity modeling in the aerodynamic analysis during optimization. This modeling is specifically applied to the wave and drag to lift terms and a brief description of simple and detailed models for each of these drag follows.

An estimation of the wave drag of the wing is provided by an algebraic model given in [39]. This model is based on theoretical and empirical studies. The algebraic model is based upon a trapezoidal wing, where the planform description is limited to the leading and trailing edge sweeps, the taper ratio, and the aspect ratio. Since the exact description of the aircraft planform is more complex then this simple description, an equivalent trapezoidal wing is utilized with the algebraic model. The details of this approximation can be found in [37].

The detailed wave-drag estimates are calculated using the classic Harris wave-drag program, [40]. This program numerically computes the value of the far-field integral arising from slender-body theory, and is known to adequately predict the wave drag of supersonic transport-class aircraft.

Figure 6.5 depicts the wave drag for both the simple and Harris code results over a varying wing geometry. This geometry is defined by a vector of design parameters p, which is linearly varied from some initial point ($\xi = 0$), to a final configuration ($\xi = 1$). The value of any given design parameter, p_i, is given by

$$p_i(\xi) = p_i(0) + \xi[p_i(1) - p_i(0)], \tag{6.1}$$

where the initial configuration is defined by the parametric description of the AST3I given in Fig. 6.2, and the final configuration is the "case 1" results which will be discussed in the following section.

The simple algebraic model for the wave drag is within 10% of the results for the more detailed Harris model although the algebraic model does not correctly predict the slope. Note that the Harris code results are not smooth. While this presents little problem for the calculation of wave drag at a given configuration, it is clear that this type of behavior will make derivative-based approximations of the detailed model such as linearization or Global-Local Approximation unreliable. Note that the algebraic model gives smooth results with reliable derivatives.

A simple model for the drag-due-to-lift term is provided by utilizing analytical results obtained for linearized supersonic thin-airfoil theory, [41]. As with the wave-drag approximation, these analytic estimates are only available for a simplified planform. In this case the simplified planform is an arrow wing where the geometrical description consists of the leading and trailing-edge angles. Once again

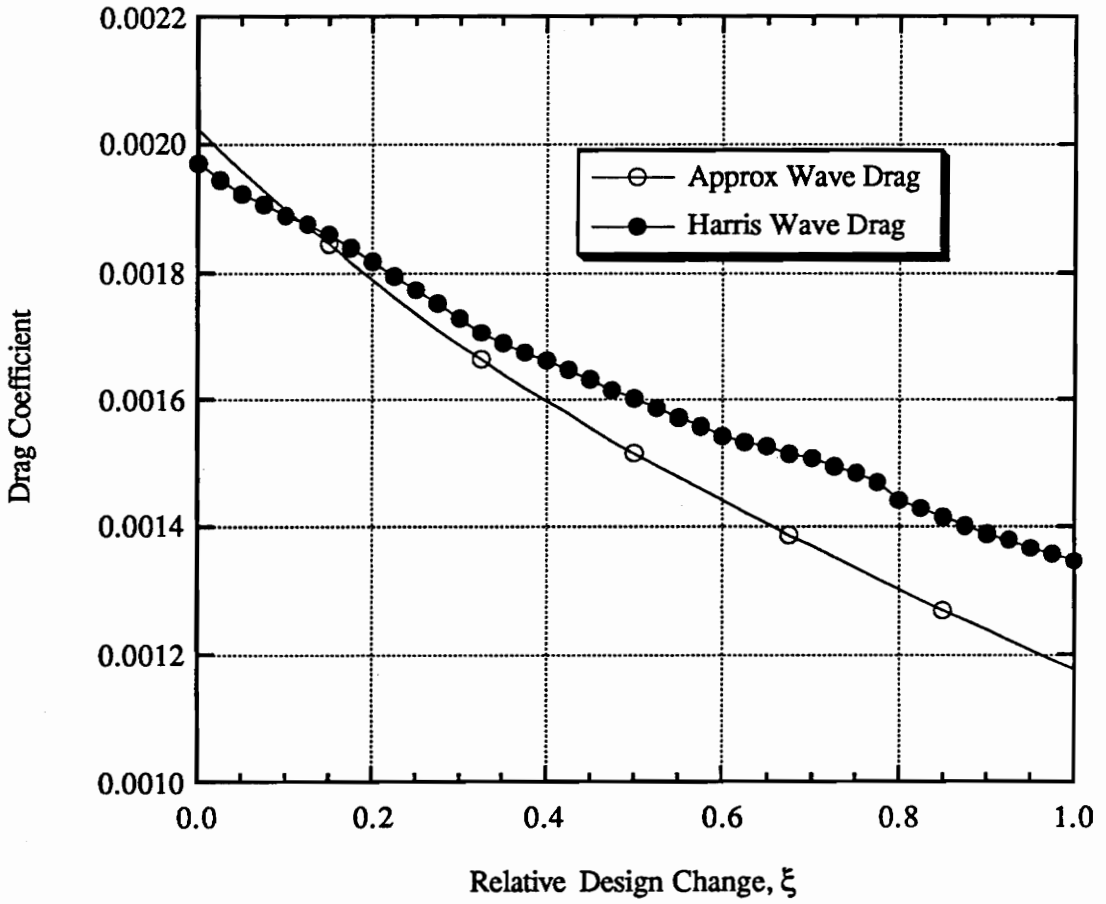

Figure 6.5. Detailed and Simple Wave Drag Model Comparisons for HSCT Design

it is necessary to provide an equivalent wing to the more general geometry for approximation purposes (see [37] for details).

The more detailed drag due to lift analysis is provided by the techniques developed by Carlson *et al.*, [42–44] and implemented by Hutchison [37]. In this approach, a panel method is utilized for the integral solution to the linearized supersonic potential equation, including the effects of attainable leading edge suction. The approach can be applied to wings of arbitrary planform.

Figure 6.6 depicts the drag due to lift for arrow wing and panel code results

over a varying geometry. The variation of the geometry is once again defined by the linear variation of the design parameters from the AST3I configuration to the case 1 design. For this case we see that the approximate model is not as accurate as the approximation for the wave drag, but we do see that is does a much better job of approximating the slope of the panel code. Note that once again the detailed model has a considerable amount of *noise* in the results. In fact, the noise for the panel code is worse than that of the Harris code.

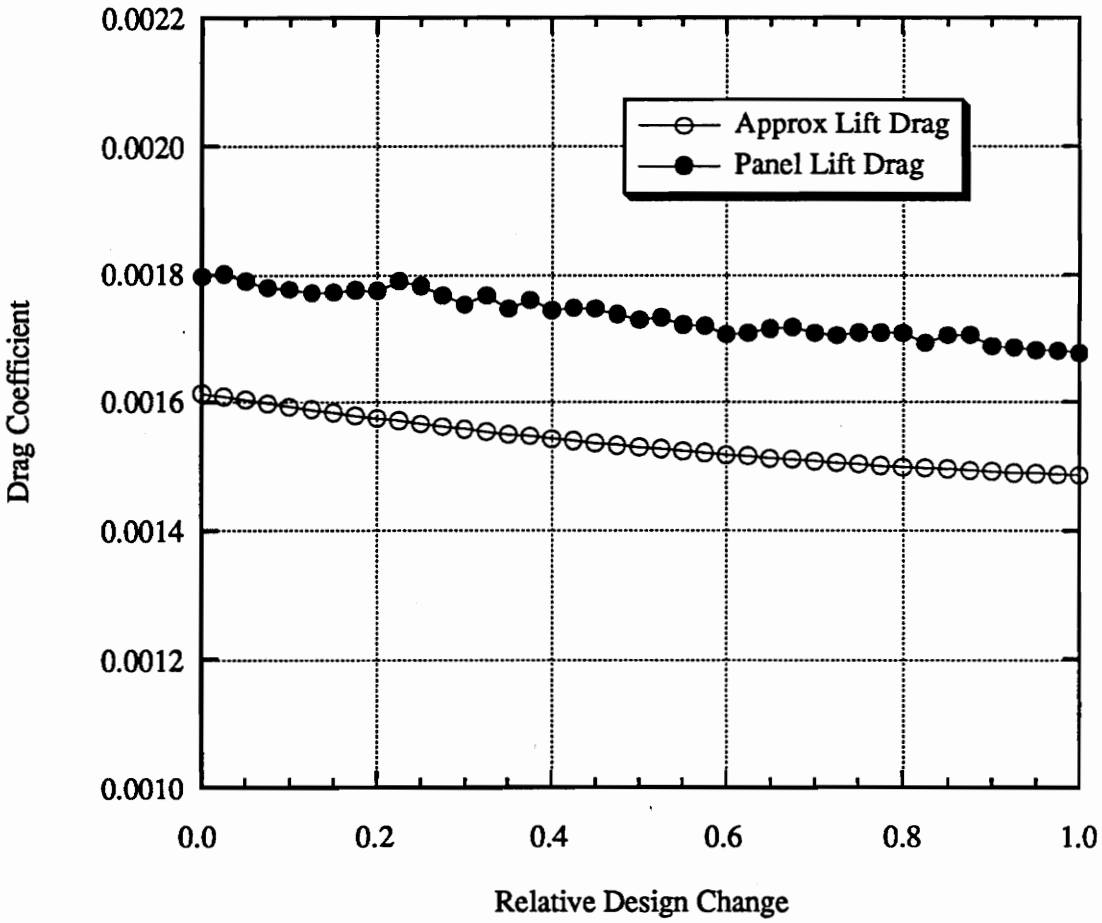

Figure 6.6. Detailed and Simple Drag-Due-to-Lift Model Comparisons for HSCT Design

The friction-drag component utilizes a single model approach with standard

algebraic estimates. The flow is assumed to be turbulent, and the so-called van Driest II method is used, as recommended by Hopkins and Inouye [45], based on an extensive set of evaluations.

6.3. Sequential approximate optimization procedure

In this example an integrated variable-complexity approach is utilized in the optimization sequence. With variable-complexity modeling a choose between Scaled and Global-Local approximation for both the wave drag and drag do to lift must be made. In general, this choice is based on which model gives the most accurate approximation in the least amount of computational effort. To such an assessment it is necessary to plot the predictions of both models verses the detailed models. Figure 6.7 illustrates such a comparison for the wave drag models on a linearly varying set of design variables as described in the previous section. The initial and final planforms for this variation are given in Fig. 6.8 which represents a maximum design variable change of 7%. From this comparison it is clear that the scaled approximation provided an approximation that was at least as good as the GLA or linear approach without the need for any detailed model derivative evaluations. This data strongly supports the use for scaled approximation, at least over this particular part of the design space. Note that for other variations of design parameters, scaled approximation may not be the most accurate choice.

Figure 6.7 also illustrates the difficulties with noisy analysis. In both the linear and GLA approaches we see that the approximation is not tangent to the detailed model at the initial design point ($\xi = 0$) as they should be. This error exists because the noise makes a finite-difference evaluation of the gradient for the detailed model (f_d') inaccurate. A considerable amount of effort was spent on refining the finite-difference approximations to improve the accuracy of the gradient evaluation. This work met with limited success and no approach was found to be very robust.

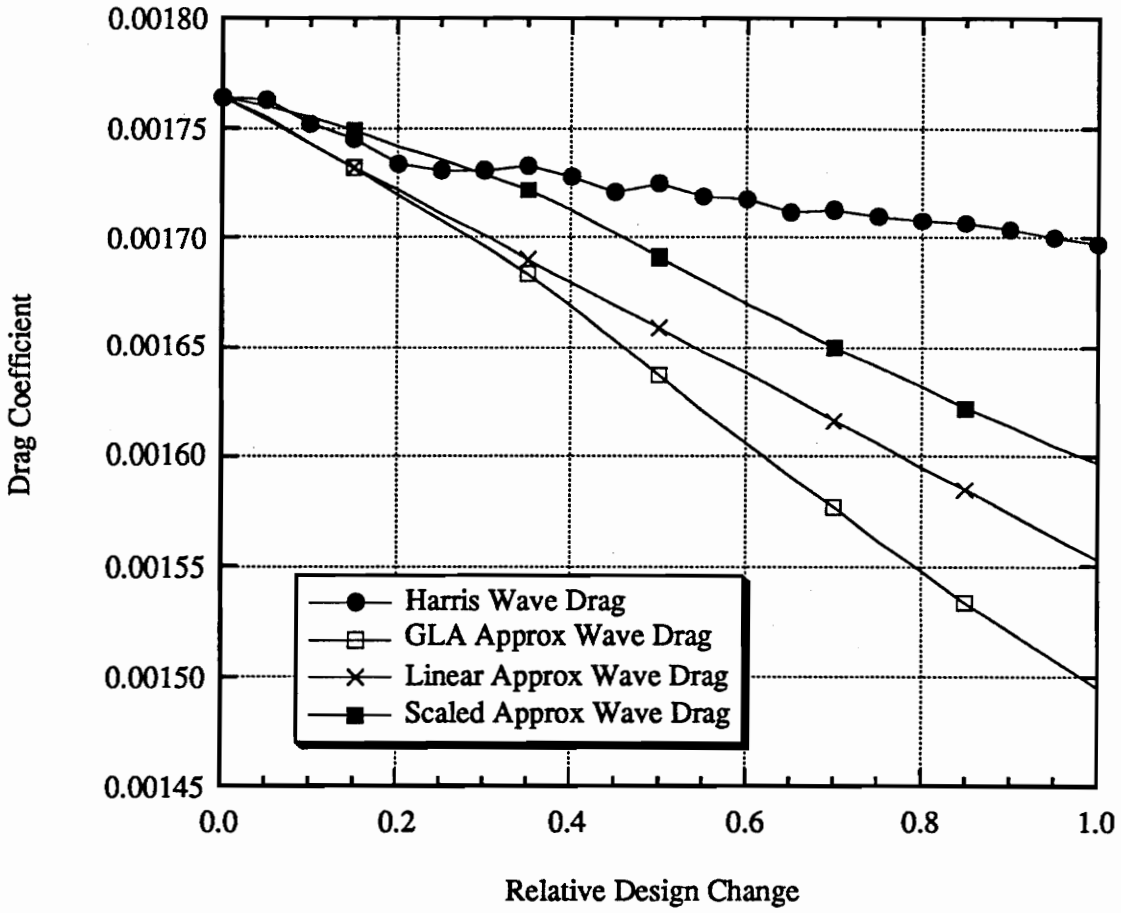

Figure 6.7. Wave Drag Approximation Strategies for HSCT Design

The approximation strategies for the drag-due-to-lift term are given in Fig. 6.9. Once again the scaled approach provides the best approximation. Note that the greater noise in the panel results make the linear the GLA approaches even worse than with the wave drag results.

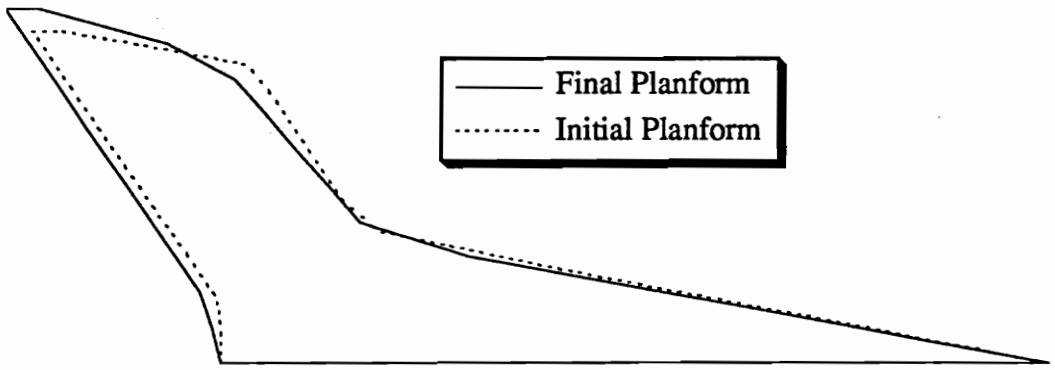

Figure 6.8. Two Configurations for HSCT Planform Used for Approximation Checks

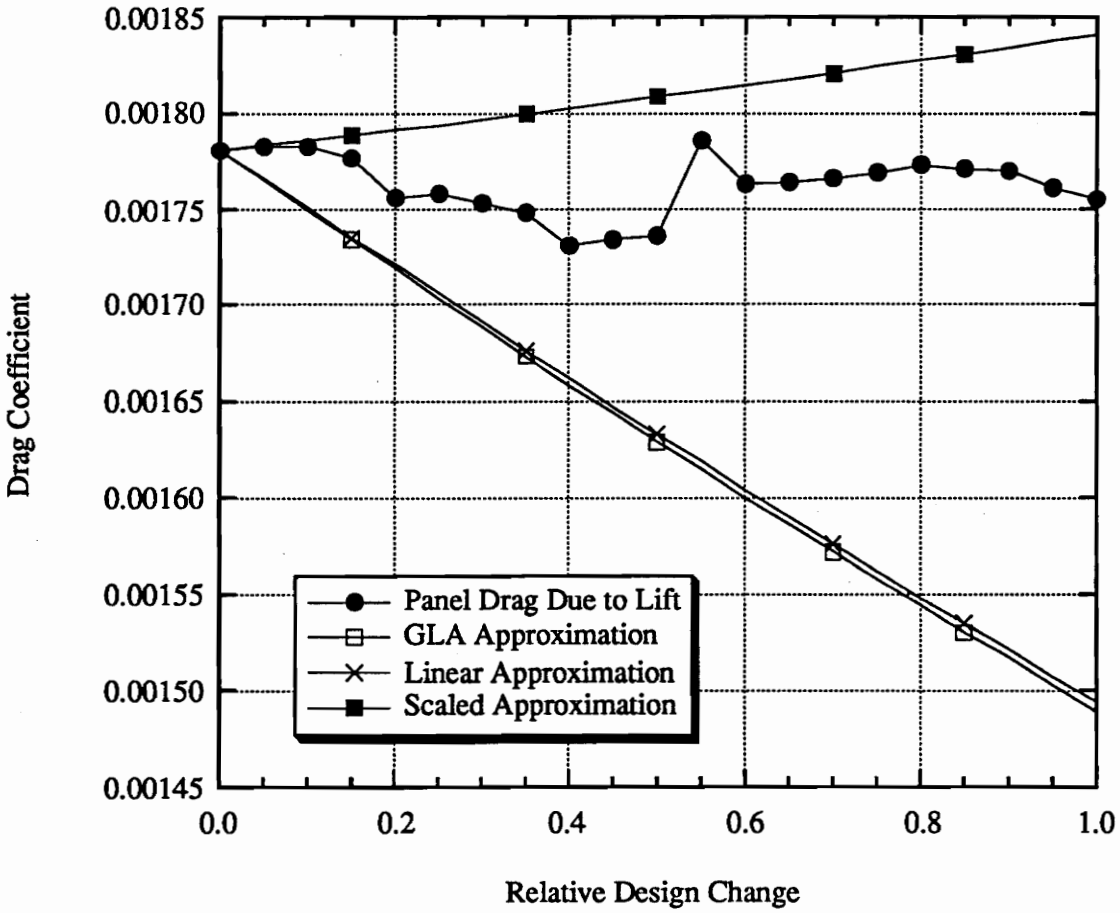

Figure 6.9. Drag-Due-to-Lift Approximation Strategies for HSCT Design

The optimization for this problem was formulated as:

$$
\begin{aligned}
\textit{minimize} \quad & W(p) \qquad (6.2)\\
\textit{such that} \quad & V(p) \geq V_r, \\
& C_{L_a}(p, W) \leq 1.0, \\
& \alpha_{L_a}(p, W) \leq 12.0°, \\
& R_c(p, D) \geq 6500mi, \\
& h_{max} \leq 70,000ft, \\
& c_l(p, y) \leq c_{l_{max}}, \\
& c(p, y) \geq c_{min}, \\
& t/c(p, y) \geq t/c_{min}, \\
& g_w(p) \leq 0 \\
\textit{where} \quad & D = D_f + \beta_w(p_0)D_{w_s} + \beta_l(p)D_{l_s}, \\
\textit{and} \quad & \beta_l(p) = \beta_l(p_0) + \beta_l'(p_0)(p - p_0).
\end{aligned}
$$

The quantities V and V_r are the available wing volume and the required fuel volume, respectively. The quantities C_{L_a} and α_{L_a} are the approach lift coefficient and angle respectively. The calculated range, R_c, depends upon the total drag of the aircraft and is required to be greater than 6500 miles. The range constraint is calculated using the exact range relationship with the approximation to the drag as where D_{w_s} and D_{l_s} give the wave and drag-due-lift results from the simple approximate models. The term h_{max} gives the maximum cruise altitude and the terms for c_l, c, and t/c provide the limitations for the local lift coefficients, chords, and thicknesses at each span location (hence the dependence on y). The final term g_w represents other wing geometric constraints such as the root trailing-edge sweep angle and the breakpoint ordering. Once again the optimizer utilized was NEWSUMT-A.

6.4. Optimization results

Two wing designs were developed from the initial configuration. The first configuration, called the "case 1" design, satisfies the constraints in Table 6.3. The second configuration, referred to as the "case 2" design, satisfied all the constraints of case 1 with the exception of the trailing-edge geometric constraint. No constraint was placed on the root trailing-edge sweep in case 2. The case 1 and case 2 planforms are presented in Figs. 6.10 and 6.11. Representative subsonic and supersonic leading edge airfoils from the initial and final designs are shown in Figs. 6.12 and 6.13. The stations at which the airfoil sections were examined were 35% and 75% of the semi-span.

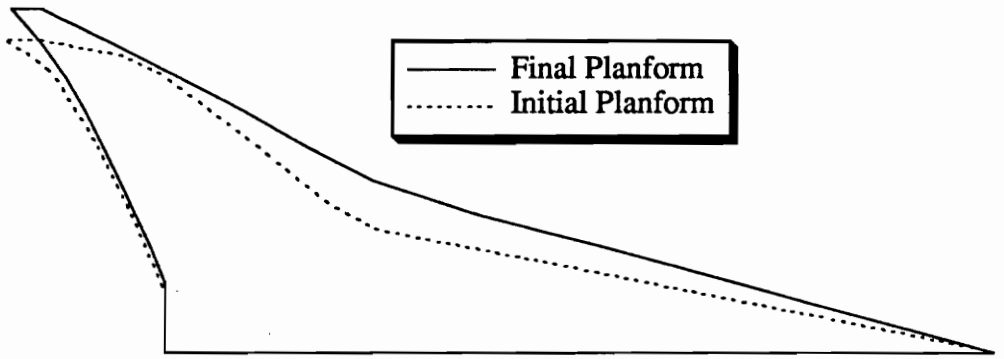

Figure 6.10. Initial and Final Planforms for Case 1

The case 2 design process was also different from the case 1 design process in the sequence of approximations chosen. At the 8^{th} iteration, the scaled approximation was utilized for the drag due to lift calculation rather than the GLA used in case 1. At the 13^{th} iteration, the constraint on root trailing-edge sweep was relaxed to allow negative sweep values. As will be shown subsequently, the performance differences between case 1 and case 2 were small.

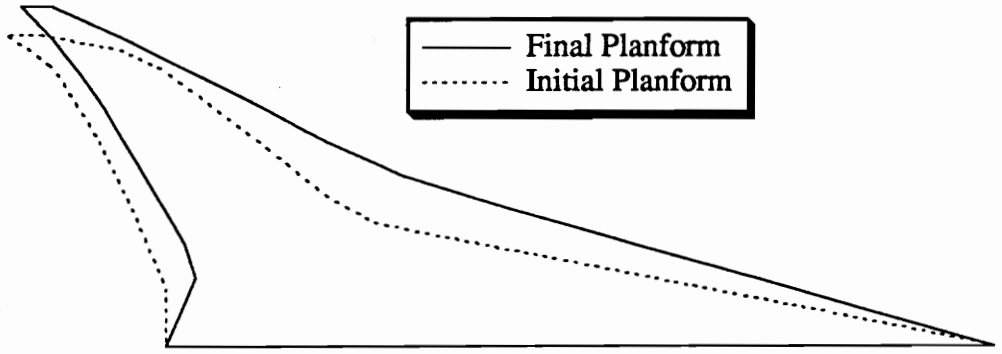

Figure 6.11. Initial and Final Planforms for Case 2

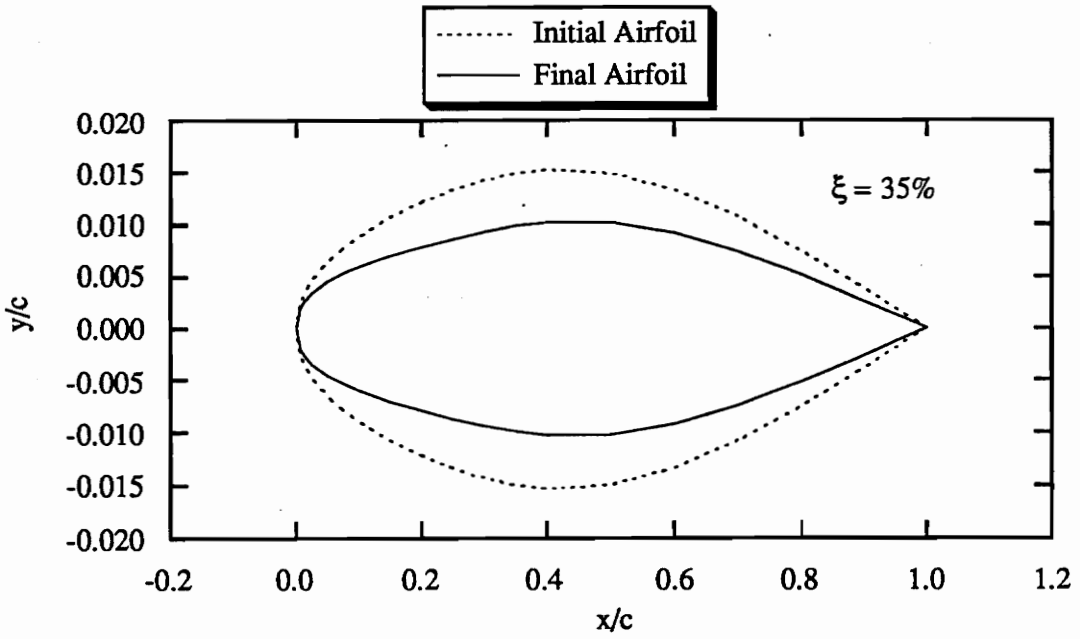

Figure 6.12. Subsonic LE Airfoil Thickness Distribution for HSCT Design

The move limits and the drag approximation methods employed in the two design sequences are shown in Table 6.4. This schedule was the result of significant experimentation and was driven largely by the difficulties associated with approximation errors in the drag estimation. At first glance, the use of Global-

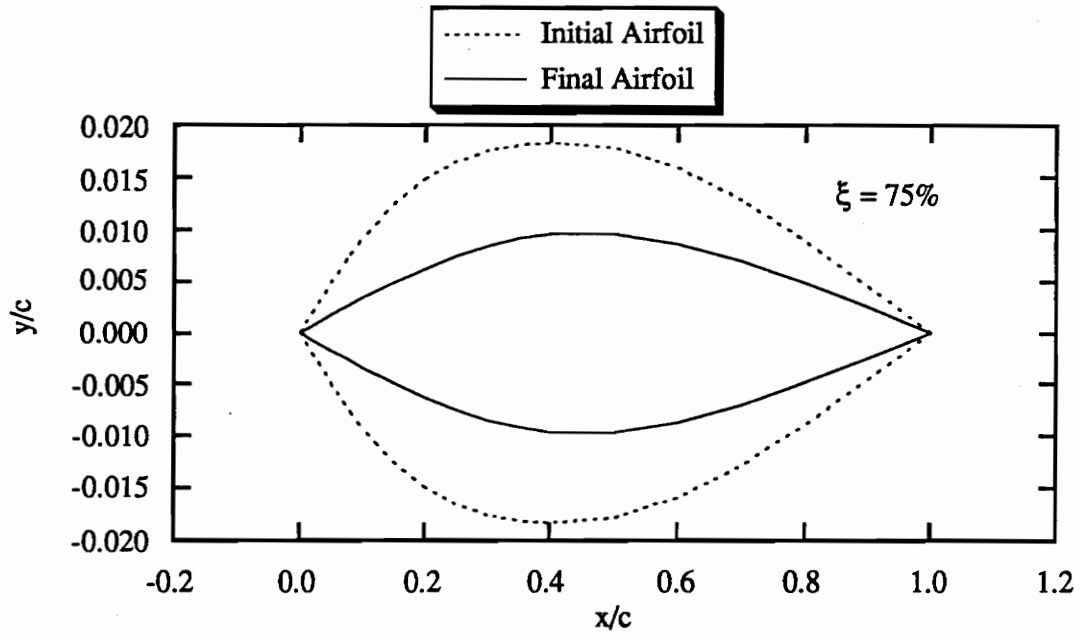

Figure 6.13. Supersonic LE Airfoil Thickness Distribution for HSCT Design

Local approximation for the drag due to lift during the initial optimization cycles may seem inconsistent with the results found in the previous section. However, this use of the GLA approach at these cycles consistently produced an optimum in the smallest number of optimization cycles. Note that poor derivatives do cause a problem with the GLA approach near convergence, and it was necessary to use the scaled approach at that point.

Of all the constraints employed, only three were active at the conclusion of the optimization. They were the landing angle-of-attack limitation, the range constraint and the altitude limitation (For case 1, the root trailing edge sweep was also active). In our early work we had not included consideration of the landing angle of attack, and obtained wings of low aspect ratio that were similar to highly-swept delta-wing planforms. The landing-angle requirement drove both wing area and aspect ratio to higher levels.

Table 4. Optimization Schedules

Cycles	Move Limits	Drag Approx Wave	Drag Approx Lift
Case 1:			
1–3	7%	Scaled	GLA
4–7	5%	Scaled	GLA
8–10	3%	Scaled	GLA
11–13	2%	Scaled	Scaled
14–18	1%	Scaled	Scaled
Case 2:			
1–3	7%	Scaled	GLA
4–7	5%	Scaled	GLA
8–10	3%	Scaled	Scaled
11–12	2%	Scaled	Scaled
13*–20	1%	Scaled	Scaled

* Trailing edge constraint removed

Figures 6.14 and 6.15 present convergence histories of the designs for aircraft gross weight and range. The oscillations in both range and gross weight due to the drag approximation errors are apparent in both figures.

The initial design represents an evaluation of the parametric model of the AST3I using the methods described above. Table 6.5 presents some details of the initial and final designs. The final designs not only weigh less, but meet the range and landing angle-of-attack requirements. The principal changes made to the initial design were to decrease the inboard leading-edge sweep and to increase the outboard sweep and the reduction in wing thickness. For example, the wing area in case 1 was redistributed inboard compared to the baseline configuration and was increased by 17.4%. The span was increased by 9.8%.

The tendency in the designs was to trade increased wing weight (thinner, larger wings) for aerodynamic efficiency (decreased wave drag) to save mission fuel. As

Table 6.5. Initial and Final Designs

	Initial Design	Optimum Design Case 1	Optimum Design Case 2
Weights (lbs$\times 10^5$)			
Gross Weight	788,600	757,400	757,500
Wing Weight	92,400	104,900	103,700
Fuel Weight	400,000	357,900	359,200
Range Margin (%)	-2.35	0.32	-0.06
Landing Angle Margin (%)	-20.4	0.00	0.00
Sweep (deg)			
Inboard LE	79.56	76.02	75.18
Outboard LE	53.13	59.85	61.79
Inboard TE	0.00	0.00	-24.33
Outboard TE	27.14	26.61	32.06
Thickness (% t/c)			
Root	2.000	1.903	1.886
LE Break 1	3.500	2.058	2.129
LE Break 2	3.500	1.902	1.960
Tip	3.500	1.894	1.950
Span (ft)	150.6	163.8	163.4
Wing Area (ft^2)	12,230	14,360	14,250
Aspect Ratio	1.854	1.869	1.873
L/D Max	7.900	8.865	8.795

* Some constraints violated

may be seen in Table 6.5, the wing weight increased while fuel weight decreased for a net savings. Figure 6.16 presents a weight breakdown of the initial and final designs. The differences between the case 1 and case 2 designs are slight. The case 1 design utilized greater aerodynamic efficiency at the expense of wing weight to achieve a minimum gross weight, while the case 2 design decreased wing weight at the expense of performance to obtain a nearly identical gross weight.

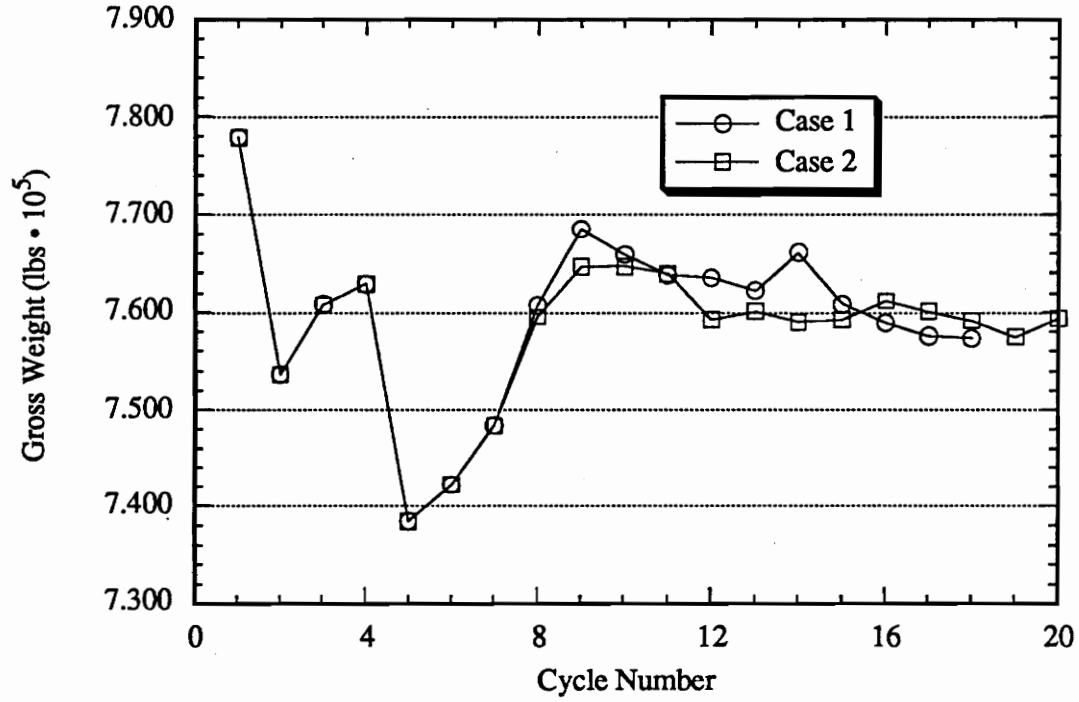

Figure 6.14. Weight Convergence History for HSCT Design

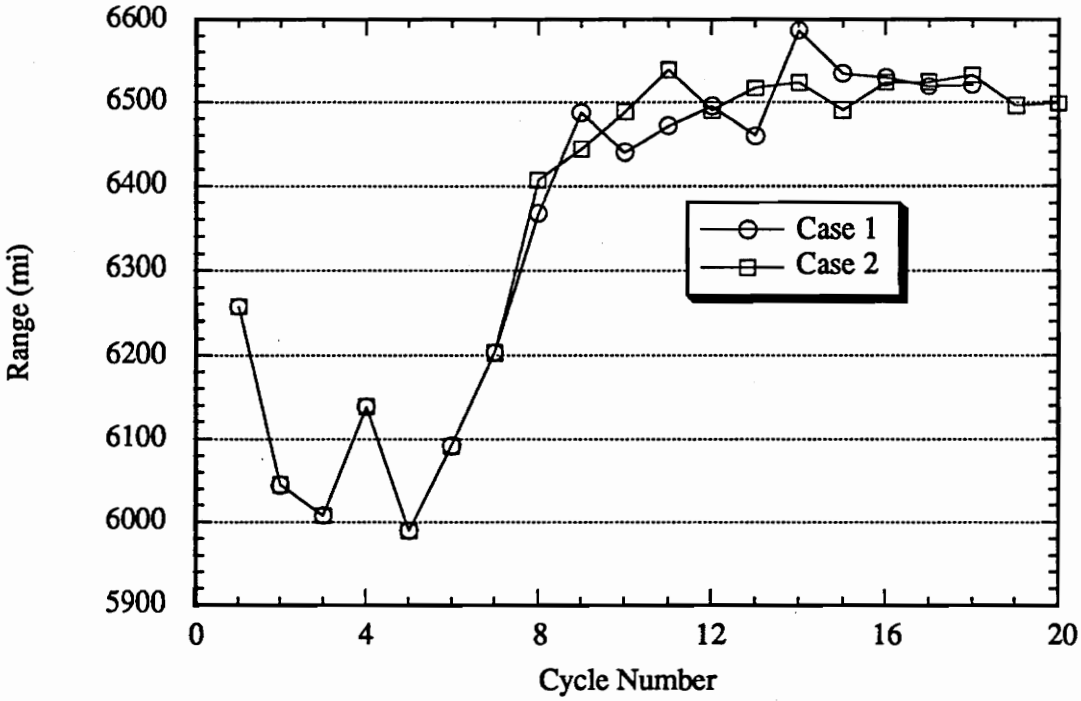

Figure 6.15. Range Convergence History for HSCT Design

Aerodynamically, the final configurations show improvements in wave drag and drag due to lift. Fig. 6.17 shows drag breakdowns for the aircraft at the start of cruise. In Fig. 6.18, the lift-to-drag ratios are presented for the initial and final designs. There was an increase of 12.2% in the maximum L/D ratio from the initial to final case 1 designs. Of this increase, approximately 70% was achieved through reductions in C_{D_0} and the remaining 30% in drag due to lift. The points corresponding to start and end of cruise are indicated. While the aircraft flies close to the maximum L/D ratio, the altitude limitation restricts the ability to fly a more nearly optimal cruise profile.

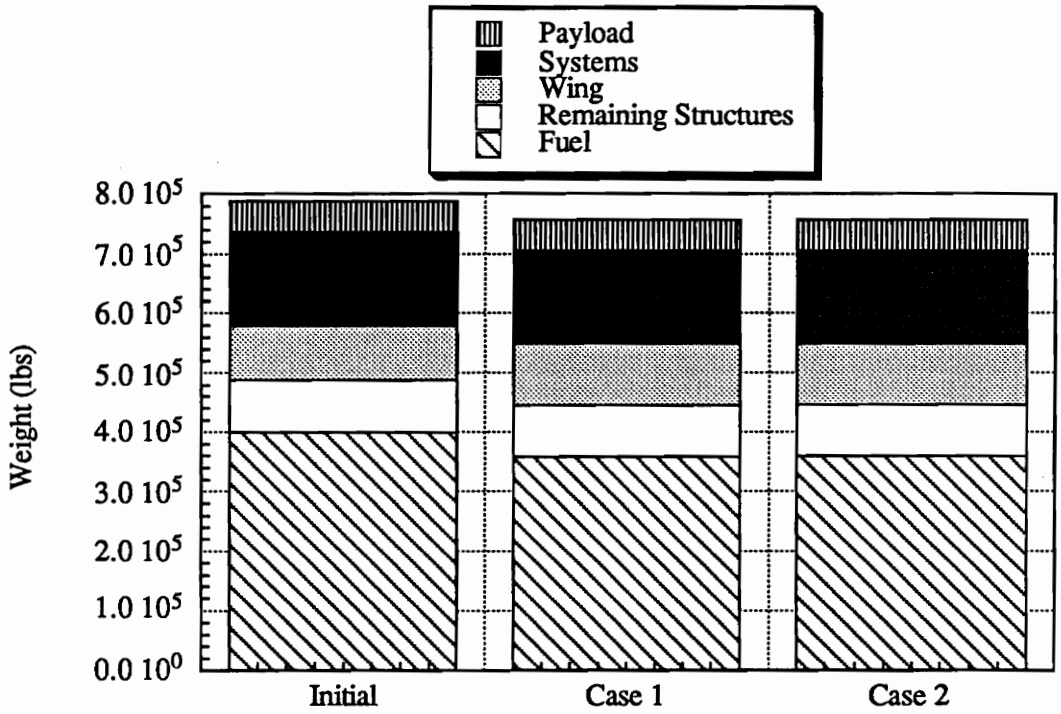

Figure 6.16. Weight Breakdowns for HSCT Design

Figure 6.17. Drag Breakdowns for HSCT Design

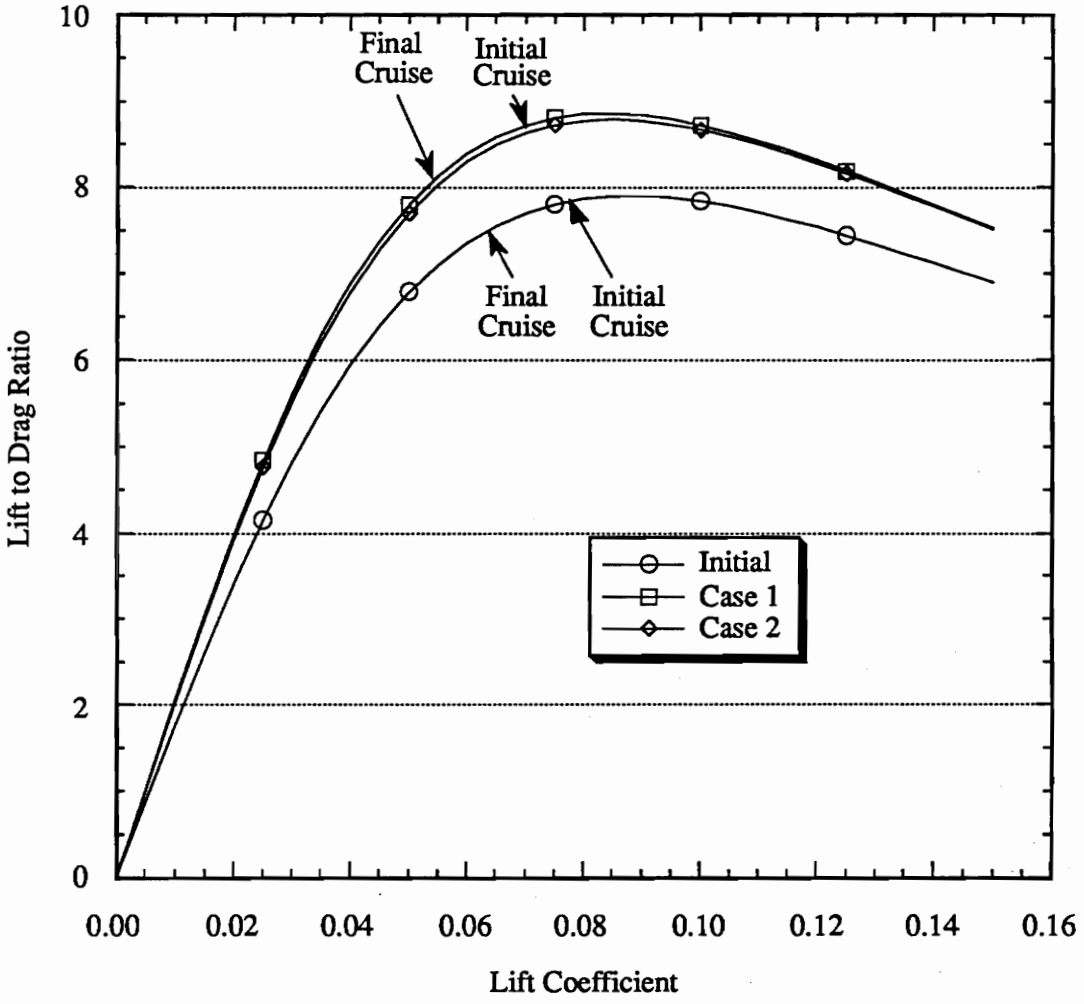

Figure 6.18. Lift to Drag Ratios for HSCT Design

7. CONCLUSIONS

Several procedures for the simultaneous aerodynamic-structural design optimization of aircraft wings have been investigated. Included in the presentation are efficient methods for optimization and sensitivity calculations which have been applied to two specific design examples. The first of these examples was a subsonic transport aircraft with a composite forward-swept wing. The aerodynamic modeling for this case was provided by vortex-lattice theory and the structural model initially utilized finite-element analysis. Although efficient methods were used in the calculation of sensitivity terms, a large amount of computational effort was still required. The majority of this cost stemmed from the large number of optimization cycles required for convergence. Since an improved initial design would reduce the number of required optimization cycles, a variable-complexity model for the structural analysis was introduced. First, an algebraic equation model for wing weight was used in the optimization procedure to obtain an aerodynamic design that approximately accounted for the effects of wing geometry on wing weight. This design was then refined by simultaneous aerodynamic-structural optimization based on the finite-element analysis. The goal of the simplified (or aerodynamic)

optimization was to provide an initial design close to the optimum of the combined aerodynamic-structural design problem. The net effect of this dual structural model was a substantial reduction in the number of iterations required for optimization and a CPU cost reduction of 75% in the best case.

The second example to be considered was the wing design of a supersonic High-Speed Civil Transport (HSCT). For this case, the simple wing-weight equations for structures were retained. For the aerodynamics, a variable-complexity model was introduced with the combination of detailed and simplified analyses for wave drag and drag due to lift during the optimization procedure. The detailed wave drag calculations were provided by volumetric wave drag analysis and the drag due to lift analysis was provided by supersonic panel methods. The simplified wave drag estimates utilized algebraic equations derived from empirical studies, and the simplified drag-due-to-lift terms utilized linearized supersonic theory for thin wings. These simplified analyses were utilized during each of the optimization cycles to minimize the number of detailed-model sensitivities required, thus reducing optimization costs.

Future possibilities exist for both the subsonic and supersonic transport examples. For the subsonic case, work has continued to include active control systems (M. Rais-Rohani [15]). However, the focus of future work at Va. Tech will be on the HSCT where a variable-complexity model for structural optimization is progressing. This work will lead to the eventual integrated aerodynamic-structural optimization of that vehicle as with the subsonic transport example. The differences between subsonic and supersonic optimization cases will be the increased use of variable-complexity techniques for the HSCT along with the use of vibration-mode analysis as opposed to the load-set approach in the subsonic case.

Future interests for the author lie in the use of non-linear CFD analysis methods during optimization for the aerodynamic predictions. The goal of utilizing these more complex methods will be to obtain more realistic final designs that account for non-linear aerodynamic behavior. The huge cost differences between CFD methods and panel approaches will require a substantial utilization of variable-complexity methods along with the utilization of parallel computer architecture. The use of parallel machines will invite the use of different approximation techniques that are generally very expensive in a single processor environment (*e.g.* Response Surface approaches [46]).

8. REFERENCES

1. Haftka, R.T., "Structural Optimization with Aeroelastic Constraints – A Survey of US Applications", *International Journal of Vehicle Design*, **7**, pp. 381–392, 1986.
2. Zeiler, T.A., and Weisshaar, T.A., "Integrated Aeroservoelastic Tailoring of Lifting Surfaces," *Journal of Aircraft,* **25**, pp. 76–83, January 1988.
3. Grossman, B., Strauch, G.J., Eppard, W.M., Gürdal, Z., and Haftka, R.T., "Integrated Aerodynamic/Structural Design of a Sailplane Wing", AIAA Paper 86-2623, AIAA Aircraft Systems, Design & Technology Meeting October 20-22, 1986, Dayton, Ohio.
4. McGeer, T., "Wing Design for Minimum Drag with Practical Constraints", *Journal of Aircraft*, Vol. 21, No. 11, 1984, pp. 879–920.
5. Haftka, R.T., Grossman, B., Eppard, W.M., Kao, P.J., and Polen, D., "Efficient Optimization of Integrated Aerodynamic-Structural Design," *International Journal for Numerical Methods in Engineering,* **28**, pp. 593–607, 1989.
6. Grossman, B., Haftka, R.T., Kao, P.-J., Polen, D.M., Rais-Rohani, M., and Sobieszczanski-Sobieski, J., "Integrated Aerodynamic-Structural Design of a Transport Wing", *Journal of Aircraft*, **27**, No. 12, 1990, pp. 1050–1056.

7. Unger, E.R., Rais-Rohani, M., Hutchison, M.G., Haftka, R.T., and Grossman, B., "Multidisciplinary design of a Subsonic Transport Wing", Proceedings of the Third Air Force / NASA Symposium On Recent Advances in Multidisciplinary Analysis and Optimization, San Francisco, Ca. Sept. 24-26, 1990.

8. Gallman, J.W., Kroo, I.M., and Smith, S.C., "Design Synthesis and Optimization of Joined-Wing Transports", AIAA Paper 90-3197, AIAA/AHS/ASEE Aircraft Design, Systems and Operations Conference, September 17-19, 1990, Dayton, Ohio.

9. Wrenn, G.A., and Dovi, A.R., "Multilevel Decomposition Approach to the Preliminary Sizing of a Transport Aircraft Wing", *Journal of Aircraft*, Vol. 25, No. 7, 1988, pp. 632–638.

10. Malone, B., and Mason W.H., "Multidisciplinary Optimization in Aircraft Design Using Analytic Technology Models", AIAA Paper 91–3187, AIAA/AHS/ASEE Aircraft Design Systems and Operations Meeting, September 23-25, 1991, Baltimore, MD.

11. Livne, E., Friedmann, P. P., and Schmit, L. A., "Studies in Integrated Aeroservoelastic Optimization of Actively Controlled Composite Wings", AIAA Paper 91–1098–CP, 1991.

12. Livne, E., Schmit, L., and Friedmann, P., "Exploratory Design Studies Using an Integrated Multidisciplinary Synthesis Capability for Actively Controlled Composite Wings", AIAA Paper 90-0953, Proceedings of the AIAA/ASME/ASCE /AHS/ASC 31*st* Structures, Structural Dynamics and Material Conference, Long Beach, CA, April 2–4, 1990, Part 1, pp. 97–109.

13. Sobieszczanski-Sobieski, J., "Sensitivity Analysis and Multidisciplinary Optimization for Aircraft Design: Recent Advances and Results," Paper ICAS–88-1.7.3, 16th Congress of the International Council of the Aeronautical Sciences, Jerusalem Israel, August 28–September 2, 1988, pp. 953–964.

14. Sobieszczanski-Sobieski, J., "On the Sensitivity of Complex Internally Coupled Systems," AIAA Paper No. CP–88–2378, and *AIAA Journal,* **28**, No. 1, pp. 153–160, 1990.

15. Rais-Rohani, M., "Integrated Aerodynamic-Structural-Control Wing Design", Ph.D. Dissertation, Virginia Polytechnic Institute and State University, August, 1991.

16. Karpel, M., "Reduced Size First-Order Subsonic and Supersonic Aeroelastic Modeling", AIAA Paper 90-1154-CP, 1990.

17. Shenna, Z. and Karpel, M., "Static Aeroelastic analysis using Aircraft Vibration Modes", Presented at the 2^{nd} International Symposium on Aeroelasticity and Structural Dynamics, DGLR Bericht 85-02, Aachen W. Germany, April 1985.

18. Dowell, E.H., Curtiss, H.C. Jr., Scanlan, R.H., and Sisto, F., *A Modern Course in Aeroelasticity*, Kluwer Academic Publishers, Boston, 1989.

19. Haftka, R.T., Sobieszczanski-Sobieski, J., and Padula, S.L., "On Options for Interdisciplinary Analysis and Design Optimization", *Structural Optimization* (in press)

20. Rodden, W. P., "Aeroelastic Divergence of Unrestrained Vehicles", *Journal of Aircraft,* **21**, No. 1, pp. 94–96, 1984.

21. Rodden, W. P., "Comment on *General Formulation of the Aeroelastic Divergence of Composite Swept-Forward Wing Structures*", *Journal of Aircraft*, **26**, No. 7, pp. 694–695, 1989.

22. Haftka, R. T., "Combining Global and Local Approximations", *AIAA J.*, **29**, No. 9, pp. 1523-1525, 1991.

23. Chang, K.J., Haftka, R. T., Giles, G.L., Kao, P. J., "Sensitivity-Based Scaling for Correlating Structural Response from Different Analytical Models", AIAA Paper No. 91-0925, April 1991.

24. Turriziani, R.V., "Continuation of a Study of the Effects of Advanced Technologies on the Sizing and Fuel Efficiency of a 150 Passenger 1220 nmi. Airplane", File: 3-92000/5LTR-007, January 1985.

25. McCullers, L.A., *Private communication*, 1990.

26. Sewall, W.G., McGhee, R. J., Viken, J. K., Waggoner, E. J., Walker, B. S. and Millard, B. F., "Wind-Tunnel Results for a High-Speed, Natural Laminar-Flow Airfoil Designed for General Aviation Aircraft," NASA TM-87602, 1987.

27. Moran, J., *An Introduction to Theoretical and Computational Aerodynamics*, John Wiley and Sons, Inc., New York, 1984, pp. 130–135.

28. Haftka, R.T. and Starnes, J.H. Jr., "WIDOWAC: Wing Design Optimization with Aeroelastic Constraints—Program Manual," NASA TM X-3071, 1974.

29. Karamcheti, K., *Principals of Ideal-Fluid Aerodynamics*, John Wiley and Sons, Inc., New York, 1966, pp. 562–563.

30. Unger, E.R., "Computational Aspects of the Multi-Disciplinary Design of a Subsonic Transport Wings", Masters Thesis, Virginia Polytechnic Institute and State University, March, 1990.

31. Grandhi, R.V., Thareja, R. and Haftka, R.T., "NEWSUMT-A: A General Purpose Program for Constrained Optimization using Constraint Approximations," *ASME Journal of Mechanisms, Transmissions and Automation in Design,* **107**, pp. 94–99, 1985.

32. McCullers, L.A., "FLOPS - Flight Optimization System, Version 2.0, User's Guide," PRC Systems Services Report, Hampton VA, Oct. 1986

33. McCullers, L.A., Lynch, R.W., "Dynamic Characteristics of Advanced Filamentary Composites Structures", AFFDL-TR-73-111, Vol. II, 1974.

34. Robins, A. Warner, Dollyhigh, S.M., Beissner, F.L., Jr., Geiselhart, K., Martin, G.L., Shields, E.W., Swanson, E.E., Coen, P.G., and Morris, S., "A Concept

Development of a Mach 3.0 High-Speed Civil Transport", NASA TM 4058, Sept. 1988.

35. Boeing Commercial Airplanes, "High-Speed Civil Transport Study", NASA CR–4233, New Airplane Development, Sept., 1989.
36. Douglas Aircraft Company, "Study of High-Speed Transports", NASA CR–4235, New Commercial Programs, Dec., 1989.
37. Hutchison, M.G., Unger, E.R., Mason, W.H., Grossman, B., and Haftka, R.T., "Variable-Complexity Aerodynamic Optimization of an HSCT Wing Using Structural Wing-Weight Equations", AIAA Paper 92-0212 presented at the 30th Aerospace Sciences Meeting & Exhibit, January 6–9, 1992, Reno, NV.
38. Barnwell, R., "Approximate Method for Calculating Transonic Flow About Lifting Wing-Body Configurations", NASA TR-452, April 1976, pp. 58-61.
39. Schemensky, R. T., "Development of an Empirically Based Computer Program to Predict the Aerodynamic Characteristics of Aircraft", AFFDL-TR-73-144, vol. 1, Nov. 1973.
40. Harris, Roy V., Jr., "An Analysis and Correlation of Aircraft Wave Drag", NASA TM X-947, 1964.
41. Jones, R.T., and Cohen, D., *High Speed Wing Theory*, Princeton University Press, 1960, pp. 197-202.
42. Carlson, H. W., Miller, D. S., "Numerical Methods for the Design and Analysis of Wings at Supersonic Speeds", NASA TN D-7713, 1974.
43. Carlson, H. W., Mack, R. J., "Estimation of Leading-Edge Thrust for Supersonic Wings of Arbitrary Planforms", NASA TP-1270, 1978.
44. Carlson, H. W., Mack, R. J., Barger, R. L., "Estimation of Attainable Leading-Edge Thrust for Wings at Subsonic and Supersonic Speeds", NASA TP-1500, 1979.

45. Hopkins, E.J., and Inouye, M., "An Evaluation of Theories for Predicting Turbulent Skin Friction and Heat Transfer on Flat Plates at Supersonic and Hypersonic Mach Numbers," *AIAA J.*, **9**, No. 6, June 1971, pp. 993-1003.

46. Barthelemy, J-F., and Haftka, R.T., "Recent Advances in Approximation Concepts for Optimum Structural Design", NASA TM 104032, March, 1991.

47. Appa, K., "Finite-Surface Spline", *Journal of Aircraft*, Vol.26, No.5, pp. 495–496, May 1989.

Appendix A. The Aerodynamic-Structural Interface

In multi-disciplinary analysis, separate models describe each physical process. For the work involved here, the models represented static structural and aerodynamic responses of a wing. For the subsonic transport example discussed in chapter 5, each of these models (FEM for structures and VLM for aerodynamics) has specific control points where displacements and/or forces are applied and calculated. In general, the structural and aerodynamic control points will be different. Therefore, there is a need to interface the structural load set nodes to the aerodynamic nodes so that information can be passed between the two models. For this specific problem, the interface involved the transference of displacements at the load set (structural) nodes to the aerodynamic control points, and the transference of forces from the aerodynamic control points to the load set nodes. The following illustrates the methodology used in the interface model.

Interface model

We begin begin by examining the deflections given at the load set nodes (recall that for the transport example given θ gives deflections at the load-set nodes and

$F_{aG} = F_a$ gives the forces at the load-set nodes) and realizing that shape functions can be employed to represent the deformation in functional form. With this formulation, shape functions interpolate the deflection of the load set nodes to the aerodynamic points. Other methods exist for this deflection approach, many using plate theory, [47]. Here we can take advantage of the grid structure for the load set nodes (Fig. A.1a) and transform this grid into rectangular cells (Fig. A.1b). Next, we can employ linear isoparametric shape functions given by:

$$\Psi_1 = (1-\xi)(1-\eta)/4\,, \tag{A.1a}$$

$$\Psi_2 = (1+\xi)(1-\eta)/4\,, \tag{A.1b}$$

$$\Psi_3 = (1-\xi)(1+\eta)/4\,, \tag{A.1c}$$

$$\Psi_4 = (1+\xi)(1+\eta)/4\,. \tag{A.1d}$$

The normalized coordinates, ξ and η, are defined in Fig. A.1c which shows a rectangular cell with the necessary corner nodes (which would correspond to load set nodes). With these functions, the deflection at any point p, bounded by the cell is simply given by

$$Z_p = \sum_{i=1}^{4} z_i \Psi_i\,, \tag{A.2}$$

where z_i is the deflection of the ith node, and Ψ_i is the ith shape function.

It is convenient to put the interpolation in a matrix format. This result can be obtained by making a unit perturbation at ith load set node, calculating the displacement at each of the aerodynamic nodes, and placing that result in the ith column of the interface transformation matrix, D. The displacement at each aerodynamic node is determined by first locating the cell in which the point lies, and then using the summation given by Eqn. (A.2). Once the unit perturbation is

cycled through all the load set nodes, the transformation matrix is completed and we have the vector of displacements at each aerodynamic node given by:

$$Z_z = D\theta\,, \tag{A.3}$$

where θ is the vector of deflections at the load set nodes.

The forces at each of the load set nodes, (F_a), can be determined by requiring the work done by the aerodynamic forces and the load set forces to be the same. We get

$$\theta^T F_a = Z_z^T F_z$$

$$\theta^T F_a = (D\theta)^T F_z$$

$$\theta^T F_a = \theta^T D^T F_z$$

so that

$$F_a = D^T F_z\,, \tag{A.4}$$

where F_z is the vector of forces on the aerodynamic control points.

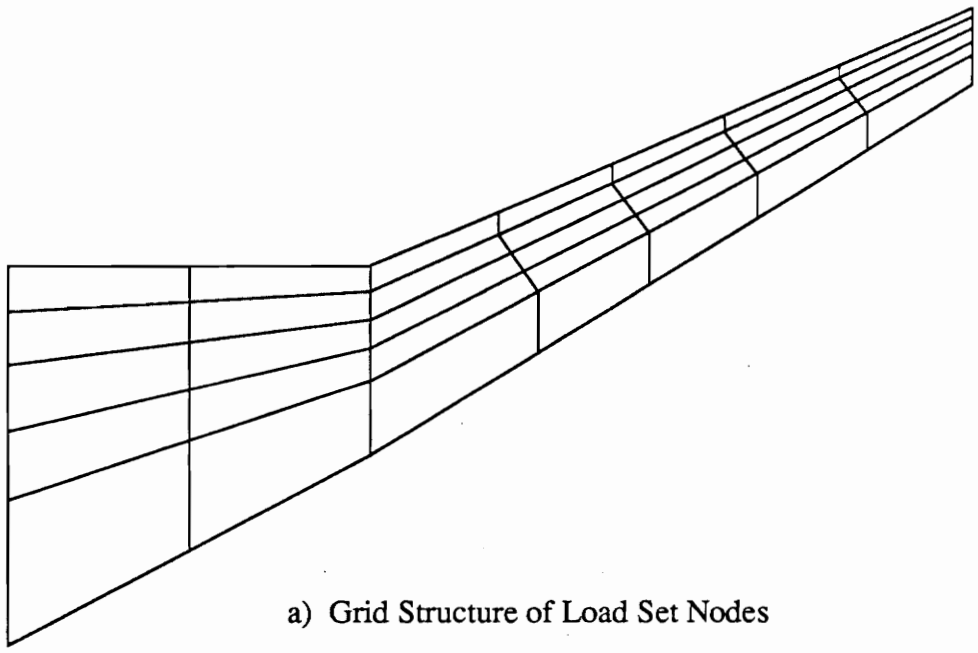

a) Grid Structure of Load Set Nodes

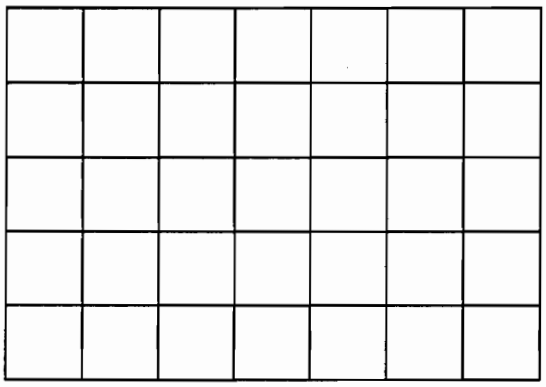

b) Transformed Grid

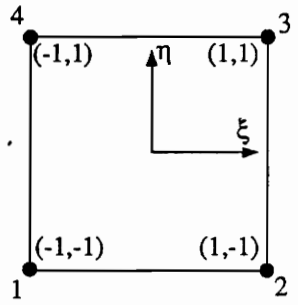

c) Interpolation Cell

Figure A.1. Load Set Grid Structure and Interpolation Cell

Appendix B. FLOPS Wing Weight Relations

The following relations detail the calculation of the wing weight as found in FLOPS, ver. 3.0, [32]. These relations have been slightly modified for our design problem.

Nomenclature

A, V	-	Beam flange cross-sectional area and volume (to be determined)
AR	-	Aspect ratio
b	-	Wing span (ft)
B_Z	-	Bending material factor (see calculations)
c	-	Airfoil chord, normalized by the wing semi-span
C_Y	-	0 if AR $\leq$ 5 , AR-5 if AR $>$ 5
f_a	-	Aeroelastic tailoring factor, [0,1]
f_c	-	Composite material factor, [0,1]
f_{UL}	-	Ultimate load factor
L	-	Total load on the wing
M	-	Wing bending moment
$p(y)$	-	Spanload on the wing, normalized by the root load
S	-	Wing area (ft^2)
S_f	-	Wing area used for flaps and control surfaces (ft^2)

t - Airfoil thickness to chord ratio
W_g - Design gross weight (lbs)
W_w - Wing weight (lbs)
y - Spanwise location, normalized by the semi-span
Λ_L - Load path angle, positive for aft sweep (spar direction)

The total wing weight (lbs) is given by

$$W_w = \frac{WCW_1 + W_2 + W_3}{1 + W_1}\,, \tag{B.1}$$

where

$$C = 8.8B_Z\left[1 + \left(\frac{6.25}{b}\right)^{\frac{1}{2}}\right] \times 10^{-6}\,, \tag{B.2}$$

and

$$W_1 = Cf_{UL}b(1 - 0.4f_c)(1 - 0.1f_a)\,, \tag{B.3}$$

$$W_2 = 0.68\,(1 - 0.17f_c)\,S_f^{0.34}W_g^{0.6}\,, \tag{B.4}$$

$$W_3 = 0.35\,(1 - 0.30f_c)\,S^{1.5}\,. \tag{B.5}$$

This system is closed except for the bending material factor. This term accounts for the load distribution on the wing. It is calculated by roughly determining the required material volume of the upper and lower flanges in the simple wing box description of the wing. We begin by finding the weighted average of the load sweep angle

$$\Lambda_{L_{avg}} = \int_0^1 (1 + 2y)\Lambda_L(y)dy\,. \tag{B.6}$$

This weighted average is based upon the observation that load sweep angles closer to the wing tip 'cost' more (in terms of weight) due to aeroelastic effects.

Next it is necessary to determine the bending moment from the supplied lift loads

$$M(y) = \int_0^y p(\xi)\xi d\xi\,. \tag{B.7}$$

With this bending moment distribution it is possible to calculate the necessary flange area as

$$A(y) = \frac{M(y)}{t(y)c(y)\cos\Lambda_L(y)}\,, \tag{B.8}$$

and the required volume as

$$V = \int_0^1 A(y)dy\,. \tag{B.9}$$

The total load is simply

$$L = \int_0^1 p(y)dy\,, \tag{B.10}$$

and the bending material factor is finally given as

$$B_Z = \frac{2V}{Ld}\,, \tag{B.11}$$

where

$$d = AR^{0.25}\left[1 + (0.5f_a - 0.16)\sin^2\Lambda_{L_{avg}} + 0.3C_Y(1 - 0.5f_a)\sin\Lambda_{L_{avg}}\right]\,. \tag{B.12}$$

VITA

The author was born in Hampton, Virginia on June 14, 1965. In 1983, he attended Virginia Polytechnic Institute and State University (VPI & SU) and entered the engineering CO-OP program. In 1988 he received his B.S. in Aerospace Engineering. Upon completion of his degree, the author married his then fiance, Susan. He then continued his education at VPI & SU to receive his M.S. Degree and Ph.D.

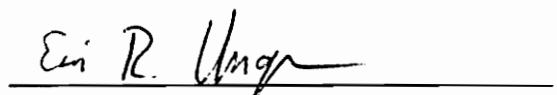

Eric R. Unger